ADVANCED QUANTUM TECHNOLOGIES
www.advquantumtech.com

Recent Advances in Quantum Effects of 2D Materials

Ya Yi, Zhanxu Chen, Xue-Feng Yu, Zhang-Kai Zhou, and Jia Li**

The celebrated discovery of graphene has spurred tremendous research interest in two-dimensional layered materials (2DLMs) with unique attributes in the quantum regime. In 2DLMs, each layer is composed of a covalently bonded lattice and is weakly coupled to its neighboring layers by van der Waals interactions. There are abundant members in this 2DLM family beyond graphene, such as transition metal dichalcogenides (MX_2, M = Mo, W; X = S, Se, Te), semimetal chalcogenide (InSe), black phosphorus, etc. The 2DLMs afford rich and ideal material platforms for studying quantum effects and their corresponding applications in the two-dimensional (2D) limit. In this review, the emerging quantum effects in 2DLMs are examined with particular focus on their band structure evolvement, valleytronics, and quantum Hall/quantum spin Hall effects. Based on the summary of quantum effects discovered in 2DLMs, the future research directions and prospective applications are also discussed.

1. Introduction

The past two decades have witnessed the remarkable triumph of 2D layered materials (2DLMs) which attract tremendous attention from both scientific and technological fields.[1] With electrons confined into an atomically thin sheet, 2DLMs provide an ideal material platform for studying quantum mechanical phenomena and applications under 2D constraints. It was not until 2004 that the freestanding, thermodynamically stable, and single-atomic layer materials were considered possible when Novoselov and Geim first isolated monolayer graphene from graphite using the simple Scotch tape exfoliation method.[2] In graphene, the unique linear dispersion relation combined with the 2D nature yields unprecedented quantum properties such as room temperature quantum Hall effect.[3] The discovery of graphene inspired and boosted the explorations of graphene-analogous 2D materials. To name a few, transition metal dichalcogenides (TMDs),[4] hexagonal boron nitride (*h*BN), black phosphorus (BP),[5] and semimetal chalcogenides (e.g., InSe) are the most extensively studied representatives. They have a similar layered structure that is stacked up and held together by weak van der Waals (vdW) forces between adjacent layers. Their properties are different and diverse due to their distinctive chemical compositions and crystalline structures. With such abundant members in the 2D materials family, not only some "traditional" quantum effects such as quantum (spin) Hall effect can be realized in these materials,[6] but also some novel quantum properties such as valley Hall effect can occur.[7] These materials-related quantum properties may open new perspectives for low-dimensional science and afford innovative concepts for devices and applications.

Essentially, the quantum effects of 2DLMs are mainly exhibited by the unique electron behaviors caused by their special structural characteristics. Specifically, the most prominent and fundamental property of 2DLMs is their ultrathin thickness, which induces various quantum confinement effects and thereby reshapes their electronic energy band struture. In addition, as the structural symmetry is taken into account, the electronic polarization of 2DLMs becomes distortive from other materials, which enables quantum technologies based on manipulating the valley degree of freedom, giving rise to applications varing from quantum communications to advanced electronics. Besides, special structural propeties also lead to unique quantum transport of electron in 2DLMs, bringing about remarkable progresses for quantum science and technology from both fundamental and applied perspectives. In this review, we will focus on the recent researches on the quantum effects of 2DLM systems, and summarize from three aspects, which are related to the three important quantum behaviors of electrons in 2DLMs (i.e., the energy band structure, polarization, and transport), respectively. The quantum-confinement induced bandgap evolution of various 2DLMs (such as TMDs, BP), valleytronics including Berry curvature, valley Hall effects, valley excitons, quantum (spin), as well as the quantum Hall effects and quantum oscillations will be introduced successively (**Figure 1**).

2. Quantum-Confinement Induced Band Structure Evolvement

In nanomaterials with dimension shaped into 2D structure, the electronic structure is significantly affected by the quantum

Dr. Y. Yi, Prof. X.-F. Yu, Prof. J. Li
Materials Interfaces Center
Shenzhen Institutes of Advanced Technology
Chinese Academy of Sciences
Shenzhen 518055, China
E-mail: jia.li1@siat.ac.cn
Prof. Z.-K. Zhou
State Key Laboratory of Optoelectronic Materials and Technologies,
School of Physics
Sun Yat-sen University
Guangzhou 510275, China
E-mail: zhouzhk@mail.sysu.edu.cn
Prof. Z. Chen
School of Optoelectronic Engineering
GuangDong Polytechnic Normal University
Guangzhou 510665, China

The ORCID identification number(s) for the author(s) of this article can be found under https://doi.org/10.1002/qute.201800111

DOI: 10.1002/qute.201800111

confinement effects (QCEs) arising from thickness reduction. For semiconducting 2DLMs, their energy gap may undergo significant changes in value and/or type (indirect or direct) with layer thickness. Due to the strong quantum confinement in the perpendicular direction, the energy bandgaps in single- and few-layer are always enlarged compared to their bulk counterparts and, in some cases, the indirect-direct-gap or direct-indirect-gap crossover may even occur.[8–10]

2.1. Transition Metal Dichalcogenides

TMDs are the most studied graphene alternatives because unlike gapless graphene, various TMD representatives are semiconductors by nature. The most prominent TMDs are the semiconducting MoX_2 (X = S, Se, and Te) and WX_2 (X = S, Se) in the 2H phase (all the Mo/WX_2 discussed in this article are in the 2H phase, if not specified). These TMDs share the similar lattice structure with a hexagonal layer of metal atoms (M) sandwiched between two hexagonal planes of chalcogen atoms (X) to form the X-M-X structure (**Figure 2**a). They possess indirect bandgaps in their bulk and few-layer forms; when the thickness decreased to single layer limit, the bandgaps abruptly turn into direct ones.[8,11,14–17] Such indirect-direct-gap crossover originates from the perpendicular quantum confinement with decreasing layer number (N). Take MoS_2 as an example, the bulk indirect-gap of 1.3 eV increases to a direct-gap of 1.8 eV in its monolayer limit, as shown in Figure 2a. The direct bandgap transition occurs between the conduction band ($c1$) and valence band ($v1$) are at the K point. The states of $c1$ at K point are composed of d-orbitals on Mo atoms; since these states are localized between two layers of S atoms, they are merely affected by the interlayer coupling. However, the indirect bandgap transition is along the Γ-K direction. The states near Γ point mainly originate from the hybridized d-orbitals on Mo atoms and antibonding p_z-orbitals on S atoms, which have strong interlayer coupling effects and much sensitive to layer thickness.[8,11] Thus, with decreasing N the strong QCEs lead to an increase of the indirect-gap, while the direct one almost remains unchanged. In monolayer MoS_2, the value of the indirect-gap at Γ point surpasses the direct one at K point, indicating the transformation into a direct-gap semiconductor. All the aforementioned 2H-MoX_2 and 2H-WX_2 are expected to experience the similar indirect-direct-gap conversion with N decreasing to one. As to WTe_2, the metallic chains of W atoms along the zigzag direction distort the ideal hexagonal lattice, leading to an orthorhombic unit cell.[18,19] Interestingly, there is a small overlap between electron and hole pockets at the Fermi surface, making WTe_2 a semimetal. Also, the closely compensated electron and hole pockets lead to an extraordinary, non-saturating magnetoresistance in both bulk and thin-film WTe_2.[20–23] Theoretical calculations predict that WTe_2 preserve the semimetal feature even down to monolayer.[24] A recent experimental work reported that the monolayer WTe_2 turned out to be a 2D topological insulator (TI) with insulting bulk and conducting edge, whereas the bilayer only become insulting without conducting edge at low temperatures (see Section 4).[25] Similarly, the 1T'-$MoTe_2$ is semimetallic in bulk with a small band overlap of 66 meV; but in few-layer, a narrow gap opening occurs in the presence of strong spin–orbit coupling (SOC), which may breed the discovery of non-trivial 2D TI in this monoclinic TMDs.[26]

2.2. Noble Transition Metal Dichalcogenides

The noble TMDs $PtSe_2$ and PtS_2 are also 2D layered semiconductors.[12,27–31] Because of the distinct crystal structure, noble-TMDs undergo a rather different layer-dependent band structure evolution, as depicted in Figure 2b. Within a $PtSe_2$ monolayer, Se atoms are strongly bonded with Pt atoms forming

Ya Yi received her Ph.D. degree from the Department of Physics at The Hong Kong University of Science and Technology in 2016. She obtained her B.Sc. degree in microelectronics at Wuhan University, China in 2012. In 2016, she joined Shenzhen Institutes of Advanced Technology, Chinese Academy of Sciences as a postdoctoral researcher. Her current research interests focus on electronics and optoelectronics based on 2D materials.

Zhang-Kai Zhou received his Ph.D. degree in physics from Wuhan University in 2011 and joined Sun Yat-sen University, Guangzhou, China, in the same year. Now he is an associate professor, as well as the deputy dean of the Department of Optics and Optical Engineering, in School of Physics, Sun Yat-sen University. His research interests mainly focus on the field of meta-optics, including quantum plasmonics, functional nanodevices based on metasurfaces, etc.

Jia Li received his Ph.D. degree in physics from the Chinese University of Hong Kong in 2009. Upon graduation, he joined the University of Tokyo, Japan, and then King's College London, UK, working as a postdoctoral researcher. He is now an associate professor at Shenzhen Institutes of Advanced Technology, Chinese Academy of Sciences. His research interests mainly focus on nanophotonics and optoelectronic devices.

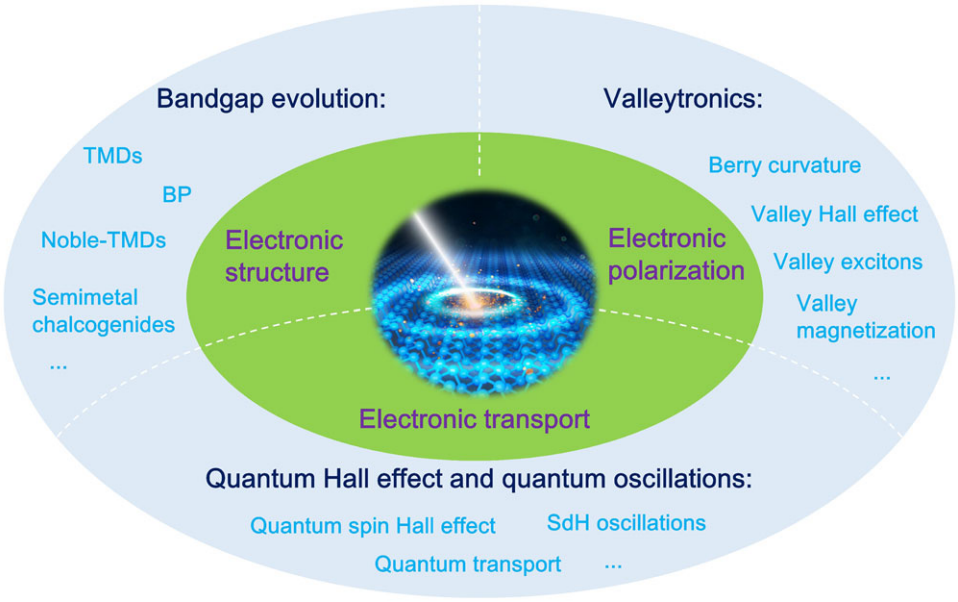

Figure 1. The outline of this review. Three main quantum behaviors of electrons in 2D materials, together with their corresponding quantum effects will be introduced in succession.

an octahedral prismatic structure.[31] The calculations show that monolayer is an indirect-gap semiconductor with energy gap value of 1.20 eV, but it decreased to a narrow gap of 0.21 eV for the bilayer counterpart; for trilayer and thicker $PtSe_2$, they become semimetallic.[30] On the other hand, the electrical transport measurements indicate that the semiconductor-semimetal transitions happen at a much thicker layer thickness (>11 nm).[31] The lattice of PtS_2 adopts a slightly distorted octahedral structure with each Pt atom in a tilted octahedral site coordinated by six S atoms.[28,29] The density functional theory (DFT) calculations reveal that PtS_2 holds an indirect bandgap from 1.8 eV of monolayer down to 0.48 eV of bulk. The bandgap values experimentally derived from the optical absorption spectra show a similar trend, that is, monotonically decrease from 1.6 eV (1L) to 0.25 eV (bulk).[28]

2.3. Semimetal Chalcogenides

Semimetal chalcogenides, such as InSe and GaSe, are a group of layered materials similar to TMDs.[14,32–39] Recently, the widely researched semiconducting InSe is in its γ phase with a rhombohedral structure.[40] As shown in Figure 2c, the primitive unit cell of γ-InSe consists of three layers, each composed of four covalently bonded Se–In–In–Se atomic planes. Within each layer, atoms form a honeycomb lattice. Bulk InSe holds a direct bandgap of ≈1.26 eV, and with decreasing thickness, the confinement effects enlarge the bandgap by ≈0.4 eV in 3-layer and more than 1 eV in monolayer, as predicted by first-principle calculations.[13,40] Moreover, with decreasing thickness (between 2- and 10-layer) the 2D InSe flakes show an indirect-gap character. This direct-indirect-gap crossover exists because of the valence band maximum (VBM) shifts about 15 meV above the valence band states at the Γ-point, where the conduction band minimum (CBM) is located. In monolayer, as Sánchez-Royo et al. noted, however, InSe is a direct bandgap semiconductor.[14] Such change in bandgap values was supported by the blue-shift in absorption edge and PL emission peak with decreasing thickness[13] (Figure 2c). Nevertheless, Sánchez-Royo et al. also mentioned that the PL quenching with decreasing thickness cannot be attributed to the direct-indirect-gap crossover, since the energy difference with respect to the Γ-point is only half of the thermal energy in room temperature.[14] Bulk GaSe is a relatively wide, indirect bandgap semiconductor (E_g ≈2.05 eV at room temperature), which previously attracted some interest because of its nonlinear optical properties.[32,33] As a 2D material, the QCEs in GaSe are not as significant as in the aforementioned materials, that is, the PL emission peak only shows a slight blue-shift of ≈30 meV with decreasing thickness from bulk to bilayer.[32]

2.4. Elemental 2D Semiconductor Black Phosphorus

The QCE-induced modification of the electronic structure with thickness reduction is also significant in elemental 2D semiconductor like BP.[41] Bulk BP possesses a direct character of the bandgap, and it keeps this direct feature down to a single layer. The QCEs in BP manifest a wide tunability of bandgap from ≈0.3 eV in bulk to ≈2.0 eV in monolayer, increased monotonically with decreasing thickness.[41–43] Actually, in monolayer BP, the VBM occurs slightly away from the Γ-point, where the CBM appears; but it is only a small deviation less than 10 meV, so it can still be considered as direct bandgap semiconductor.[44]

3. Valleytronics

Following the summary of quantum effects caused by the quantum evolution of electron energy band structure, we will

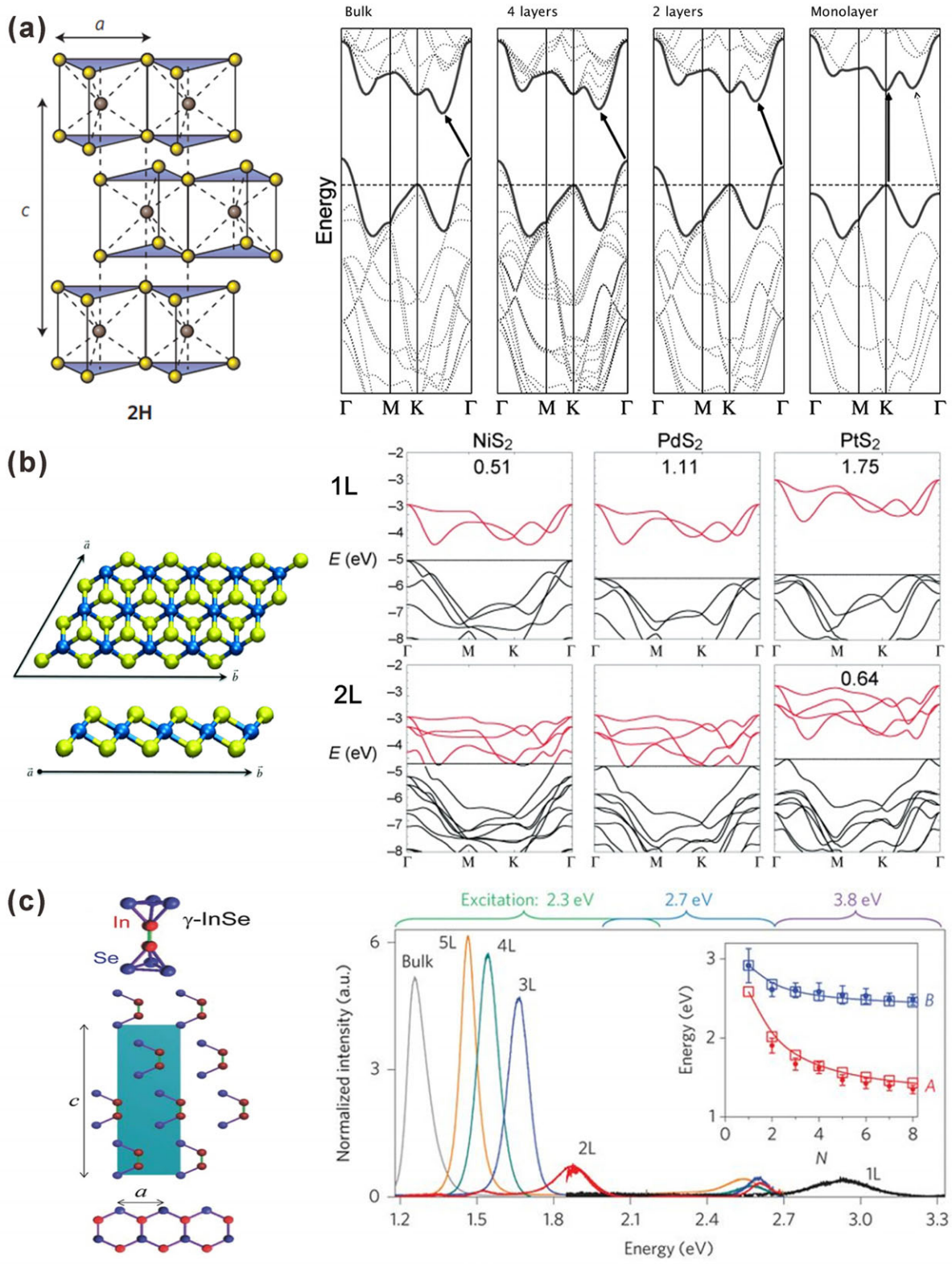

Figure 2. Evolution of the band structure of 2D semiconductors. a) Lattice structure (left) and calculated band evolution of 2H-MoS_2 with decreasing thickness (right). Left: Reprinted with permission.[10] Copyright 2012, Nature Publishing Group. Right: Reprinted with permission.[11] Copyright 2010, American Chemical Society. b) Lattice structure (left) and band structure calculated monolayers and bilayers (right) of Noble-TMDs. Reprinted with permission.[12] Copyright 2014, Wiley-VCH. c) Lattice structure (left) and PL spectra of InSe from bulk to monolayer (right). Inset: energies of peak A (low energy) and B (high energy) with different *N* (layer number). Reprinted with permission.[13] Copyright 2017, Nature Publishing Group.

introduce the quantum effects related to valleytronics. Generally, valleytronics results from special electron polarization in 2DLMs, and it is the technology of manipulating the valley quantum degree of freedom (DoF) to store and process information. Valleytronics has been attracting growing interest for the next-generation electronics and optoelectronics.[7] The valleys are referred to the local energy extrema in the momentum space. The term "valleytronics" is coined from "spintronics", since the binary valley pseudospin, which labeled the valley indices, are much analogous to the spin up and down states. The idea of valleytronics can be traced back to 1970s, when researchers proposed that the valley indices can act as an information carrier in conventional semiconductor AlAs or Si. However, such exploration had been rather limited until the recent emergence of 2D materials that host hexagonal lattice structure, such as graphene and TMDs.[7] In such material systems, the band edge electrons—in the vicinity of CBM and VBM—are confined in two degenerates yet inequivalent valleys located at the K and −K points.[45] Specifically, the electrons in K valley can be labeled as valley-pseudospin up, and those in −K valley can be labeled as valley-pseudospin down.[46] The generation, detection and controlment of valley polarization have been demonstrated through optical, magnetic, and electrical methods.[47,48] In this section, we are going to review the recent research process on valleytronics in 2D hexagonal crystals.

The valley-contrasting physical properties generically stems from the broken inversion symmetry.[45,49,50] In systems such as gapped graphene and odd-layer TMDs, the broken inversion symmetry together with the preserved time reversal symmetry (TRS) dictate the Berry curvature (**Ω**) and the valley orbital magnetic moment (**m**) to have identical magnitudes but opposite signs in these K and −K valleys. These two valley-contrasting physical quantities are useful, if not necessary, to distinguish electrons in these two valleys, leading to various valley-dependent electronic and optoelectronic properties.[51]

3.1. Berry Curvature

Let us start with the Hamiltonian in graphene and 1L-TMDs near the ±K points. Without considering the spin–orbit coupling (SOC) term, the simplest two-level Hamiltonian $\hat{\mathcal{H}}$ can be described as

$$\hat{\mathcal{H}} = a\left(\tau k_x \sigma_x + k_y \sigma_y\right) + \frac{\Delta}{2}\sigma_z$$

where a is a coefficient charactering the material, $\tau = \pm 1$ is the valley indices, $\boldsymbol{k} = (k_x, k_y)$ is the crystal momentum measured from the valley center (±K points), Δ is the bandgap ($\Delta = 0$ for graphene and $\Delta > 0$ for 1L-TMDs), and $\boldsymbol{\sigma} = (\sigma_x, \sigma_y, \sigma_z)$ is the Pauli matrices for two-band basis functions that define the band edges.[45,49,50]

3.2. Valley Hall Effect in Graphene

Indeed, the Berry curvature is a momentum space analog of magnetic field (B-field) along z-direction. It takes the expression of $\boldsymbol{\Omega}_k = \nabla_k \times u(\boldsymbol{k})|i\nabla_k|u(\boldsymbol{k})$, where u is the periodic part of the Bloch function. In opposite valleys, the Berry curvatures have opposite signs; in the same valley, the Berry curvature for valence and conduction bands also take opposite signs. Therefore, in the presence of an in-plane electric field $\boldsymbol{E}$, the moving electrons will experience a Lorentz-like force and gain an anomalous velocity $v_a = \frac{e}{\hbar}\boldsymbol{E} \times \boldsymbol{\Omega}$, where e is the elementary charge and $\hbar$ is the reduced Planck constant, giving rise to a transverse Hall current. Since v_a is proportional to $\boldsymbol{\Omega}$, the Hall current have equal magnitudes but opposite signs in these ±K valleys, as illustrated in **Figure 3**a.[45] This phenomenon is known as the valley Hall effect (VHE), which was successfully demonstrated in graphene and TMDs systems in recent years.[52,55–57] In both mono- and bilayer graphene, although their lattice structures are centrosymmetric, the inversion symmetry can be explicitly broken by introducing external perturbations. The first experimental demonstration of VHE in single-layer graphene (SLG) was reported by A. K. Geim's group in 2014.[52] By stacking SLG and hBN and deliberately aligning their crystal direction, the inversion asymmetry can be induced by the staggered sublattice potential, resulting in an opening gap and finite **Ω** in SLG. In the bilayer graphene (BLG), the inversion symmetry can be controllably broken by an external perpendicular electric field.[55,56] In both the SLG/BN superlattice and the gate-biased BLG, the direct and inverse VHEs were measured in a Hall-bar configuration, and manifest as a nonlocal resistance at zero B-field (Figure 3b). Such nonlocal signal directly arises from the topological transport of valley pseudospin and exhibits a long response length of micrometers away from the current injection end. This nonlocal response is even more robust in gate-biased BLG which can persist in room temperature,[55,56] whereas in SLG/BN the it is absent above 150 K.[52] A more recent experiment work shows that in BLG, a near-ballistic valley transport with a mean free path up to a few hundreds of nanometers can be realized by utilizing a dual-splitting-gate scheme.[57]

3.3. Valley Hall Effect in Transition Metal Dichalcogenides

For 2D TMDs, they are semiconductors by nature, which facilitate the manipulation of valley pseudospin through optoelectronic methods.[47,58] It is intuitive to envision that 1L-TMDs are readily for light coupling because of their direct and moderate bandgaps. In 1L-TMDs, the CBM mainly consists of d_{z^2} orbitals with a magnetic quantum number 0, while VBM mainly consists of $(d_{x^2-y^2} + i\tau d_{xy})$ orbitals with a magnetic quantum number of 2τ. Taken into account the valley orbital angular momentum and the C_3 symmetry of the lattice, the interband transitions follow a valley optical selection rule, where interband transitions in the vicinity of +K/−K points are exclusively coupled to right/left circularly polarized light σ^+/σ^-, analogous to the spin optical selection rule in III-V semiconductors.[45] As the light circular polarization remains unchanged under inversion symmetry, the lacking of this symmetry is necessary to ensure such a selection rule.

Bearing in mind these perspectives, it is not surprising that the first experimental demonstration of VHE in TMD systems is by performing optoelectronic measurements in a monolayer MoS_2 transistor with standard Hall bar geometry.[53] In such experiments, the net Hall voltage was attained by explicitly breaking

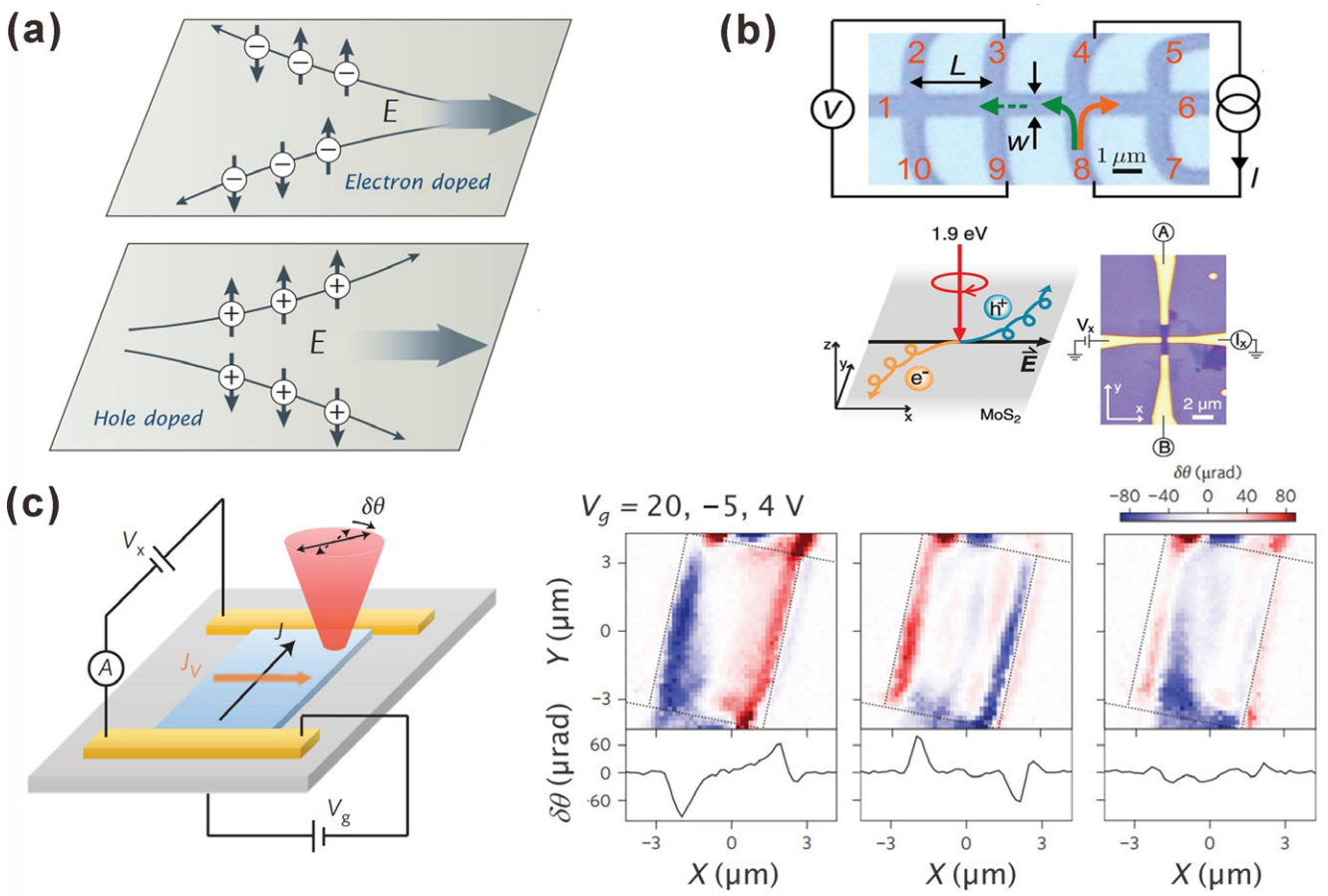

Figure 3. Valley Hall effect in 2D hexagonal crystals. a) Illustration of the valley electron/hole Hall effect when an in-plane electric field E is applied. The arrows indicate the real spin of charge carriers. Reprinted with permission.[45] Copyright 2012, American Physical Society. b) Experimental demonstration of VHE. (Top) Monolayer graphene/BN device, where I, flows between contacts 4 and 8, and a nonlocal voltage, V, is measured between contacts 3 and 9. L is the length between the Hall contacts and W is the channel width. Reprinted with permission.[52] Copyright 2014, American Association for Advancement of Science. (Bottom right) Monolayer MoS_2 Hall bar device, where V_x is along the short channel and the Hall voltage between A and B is measured. (Bottom left) Schematic of the photoinduced VHE driven by a net valley polarization. Reprinted with permission.[53] Copyright 2014, American Association for Advancement of Science. c) Experimental demonstration in bilayer MoS_2. (Left) Schematic of the Kerr rotation microscopy measurement of VHE. A valley current density J_V (orange arrow) in the transverse direction is induced by a longitudinal electrical current density J (black arrow). The VHE which was detected by focusing a linearly polarized probe beam onto the device under normal incident and measuring the Kerr rotation angle $\delta\theta$ of the reflected beam. (Right) Spatial maps of the Kerr rotation signal for different gate voltage V_g. Reprinted with permission.[54] Copyright 2016, Nature Publishing Group.

the TRS to create a net valley polarization (Figure 3b). Specifically, they selectively applied σ^+/σ^- excitation to preferably inject electrons and holes in K/−K valley, thus creating an imbalance of carrier population between two different valleys. Under an in-plane bias, the photoexcited electrons and holes acquire opposite anomalous velocities, and drift to opposite sample edges, thus generating a net transverse Hall voltage whose sign depends on the helicity of the light. Later, the observation of VHE in bilayer MoS_2 (2L-MoS_2), which is a centrosymmetric crystal, was also reported.[54] The approach is similar to the case of BLG, inversion symmetry in 2L-MoS_2 was broken by applying a perpendicular electric field. Instead of using electrical methods, the VHE in 2L-MoS_2 was directly imaged by the Kerr rotation microscopy (KRM) (Figure 3c). Because of the transverse Hall current, electrons from opposite valleys were accumulated along the opposite channel edges. Probing with a linearly polarized light, this kind of net valley polarization manifested as the different reflectance to the σ^+ and σ^- component, which was mapped as finite Kerr rotation angles with opposite signs at the two edges.

3.4. Valley Excitons

While the above discussed valley-dependent physics phenomena are considered to originate from the valley polarization of free carriers, the excitonic effects are quite pronounced in 1L-TMDs, enabling the manipulation of valley pseudospin through valley excitons (**Figure 4**a).[60,61] Owing to the reduced screening effect and the heavy particle band masses, the Coulomb interaction is remarkably strong, giving rise to the extremely large exciton binding energy in the range of 0.3–1 eV.[17,62–64] In the photoluminescence (PL) measurements performed on 1L-TMDs, as

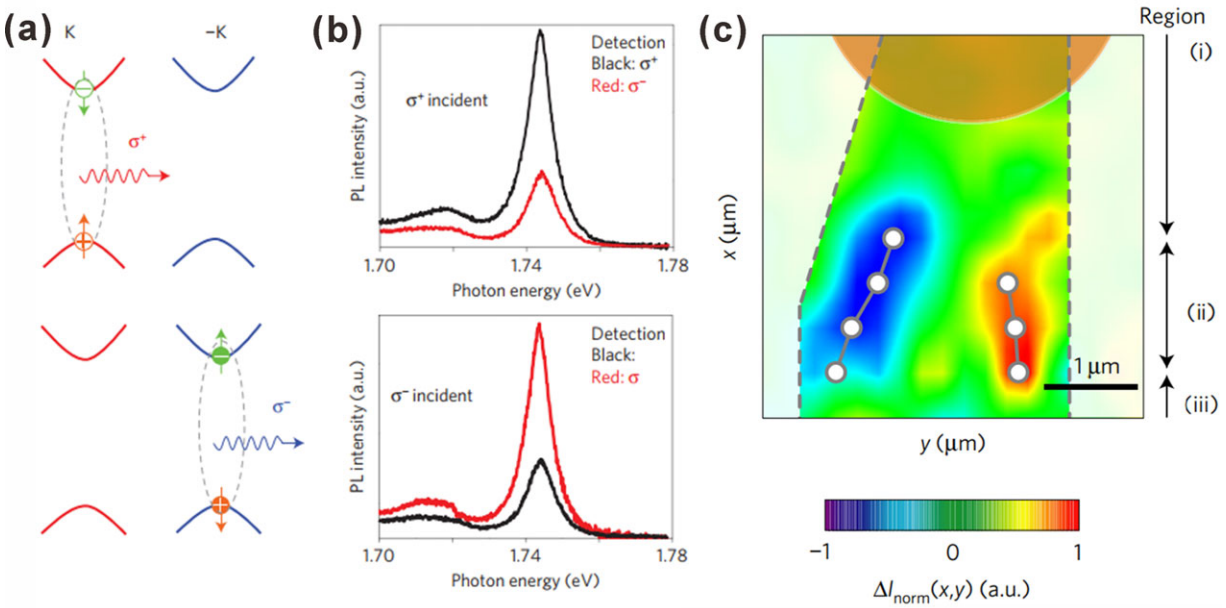

Figure 4. Valley polarization of excitons in 2D TMDs. a) Energy level diagrams with polarized emission at ±K valleys. The arrows indicate the spin of electrons and holes. Reprinted with permission.[46] Copyright 2014, Nature Publishing Group. b) Polarization-resolved exciton emission in monolayer WSe_2 by $\sigma+$ (right) and $\sigma-$ (left) excitation. Reprinted with permission.[46] Copyright 2014, Nature Publishing Group. c) Spatial map of ΔI_{norm} $(\Delta I_{norm}(x,y) = (I_{\sigma+}(x,y) - I_{\sigma-}(x,y)/I_{sum}(x))$, which exhibits the EVHE in real-space. The white circles show the peak position of ΔI_{norm}. The gray dash lines mark the edges of the flake and the orange circle indicates the laser spot. Reprinted with permission.[59] Copyright 2017, Nature Publishing Group.

shown in Figure 4b, the helicity of the PL emission was shown to have the same circularly polarized component with the excitation light.[65–68] Pumping with σ^+/σ^- and then detecting with polarization-resolved PL (σ^+ and σ^- components) intensities, the valley polarization, η, can be defined as

$$\eta = \frac{\mathrm{PL}(\sigma^+) - \mathrm{PL}(\sigma^-)}{\mathrm{PL}(\sigma^+) + \mathrm{PL}(\sigma^-)}.$$

Upon near-resonant excitation, the valley polarization η in the range of 30–100% at low temperatures (below 10 K) were reported in MoS_2, WS_2, and WSe_2 single layers.[65–68] The value of η drops dramatically with increasing temperature, suggesting a phonon-assisted intervalley scattering.[65] That the origin of this polarized PL comes from the valley spin was justified by the absence of Hanle effect, that is, the in-plane B-field can only cause the procession of real spin but not of valley pseudospin. In 1L-MoS_2, the dichroism of PL is robust under the in-plane B-field up to 9 T, unambiguously demonstrating that the PL polarization comes from valley pseudospin.[69] This is consistent with the fact that the valley magnetic moment **m** is aligned to the out-of-plane direction which cannot couple to the in-plane B-field. If the excitons are formed through electrically injected electrons and holes, the corresponding excitonic emission is called electroluminescence (EL). Using electrostatic doping to produce a p-n architecture in mono- and few-layer (Mo,W)Se_2 films, the EL shows a gate tunable circularly polarized light emission.[70–72] Recently, the exciton VHE (EVHE) in monolayer MoS_2 characterized by polarized PL mapping has been reported.[59] Under laser illumination, excitons (neutral and charged) generated in opposite valleys transversely drifted to opposite channel edges. This accumulated excitonic valley polarization was then characterized by the normalized difference between the σ^+ and σ^- components of the PL signal, manifesting as the transverse splitting of PL polarization in real-space, as shown in Figure 4c. The extracted valley diffusion length ℓ_v was of ≈2.0 μm, consistent with the spin-valley free path of electrons and holes in 1L-WS_2. Also, the ℓ_v is comparable to the exciton diffusion length ℓ_x, suggesting the robust preservation of valley polarization during transport. Moreover, the Hall angles of this EVHE is nearly two orders of magnitude larger than that of the single particles dominated VHE in 1L-MoS_2, which may arise from the internal topological nature of the excitonic states.

3.5. Valley Magnetization

The valley-dependent **m** allows the magnetic control of valley polarization. Coupling the valley pseudospin with an out-of-plane B-field, the TRS can be broken and thus the valley degeneracy can be lifted. This effect is called the "valley Zeeman effect," in analog to the real-spin Zeeman splitting under B-field. The valley Zeeman effect can be characterized by polarized PL measurements under B-fields, which is supposed to shift the transition energy for σ^+ and σ^- light in opposite directions.[73–76] In this scenario, a redshift of emission from K valleys with respect to that from −K valleys for B>0 and a blueshift for B<0 are expected. The experimental demonstration of valley Zeeman effect has been realized in monolayer WSe_2,[73,74] $MoSe_2$,[75] MoS_2, and WS_2.[76] However, such valley splitting is relatively small (≈0.2 meV T^{-1}), limiting the practical applicability and feasibility of the control of valley DoF in TMDs. Alternatively, the valley Zeeman effect can

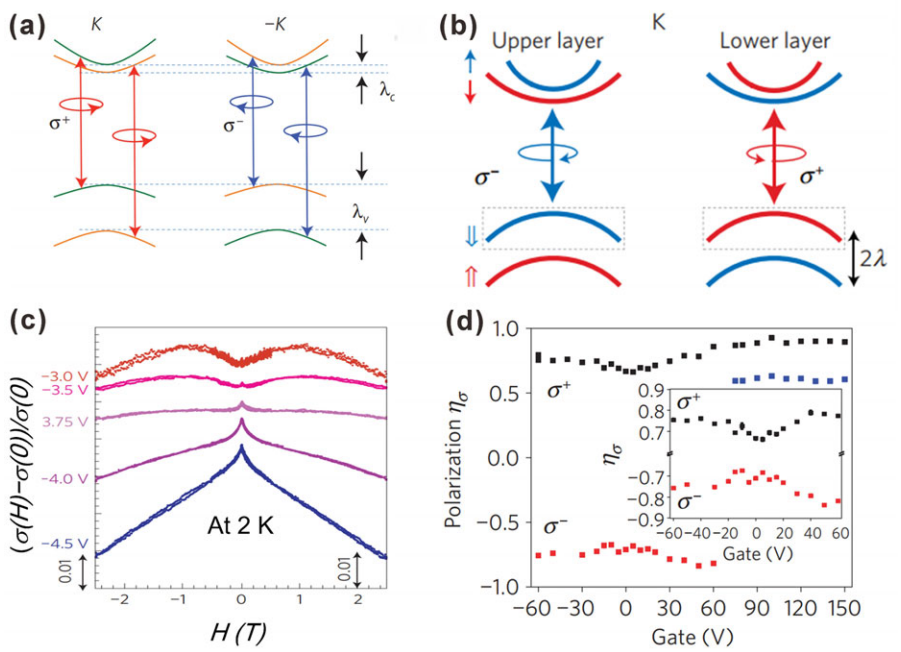

Figure 5. The interplay between real-spin, valley, and layer pseudospin. a) Spin and valley optical selection rules in monolayer TMDs. λ_c/λ_v: the spin–orbit coupling induced energy splitting in conduction/valence bands. Reprinted with permission.[46] Copyright 2014, Nature Publishing Group. b) Excitation/emission process of $\sigma+$ (right) and $\sigma-$ (left) circular polarization in the K valley of bilayer WSe_2. Single and double arrows indicate the spin configuration of electrons/holes, respectively. The same for −K valley can be obtained through time reversal. Reprinted with permission.[81] Copyright 2014, Nature Publishing Group. c) Gate (V_g) modulation of magnetoconductance in bilayer WSe_2. A clear crossover from weak localization to weak anti-localization occurs as negative V_g increases. The vertical arrows labeled "0.01" indicate the scale of relative conductance. Reprinted with permission.[82] Copyright 2013, Nature Publishing Group. d) PL circular dichroism of trions in bilayer WSe_2, η_σ, as a function of gate voltage. Black/red denotes $\sigma+/\sigma-$ excitation. For $V_g > 50$ V, the trion peak splits and black/blue data show the η_σ of two splitting peaks under $\sigma+$ excitation. (Inset) Zoom-in picture which emphasizes the enhancement of $\eta\sigma$ with V_g for both σ^+ and σ^- excitation.[81] Reprinted with permission.[81] Copyright 2014, Nature Publishing Group.

be largely enhanced in TMDs-ferromagnetic insulator hybrids. The proximity-induced exchange interaction acts as an effective magnetic field on the orders of ≈10 T (on EuS and CrI_3) that significantly enhances the valley splitting.[77,78] The generation of valley magnetization in electrically biased SL-MoS_2 by a uniaxial strain was also reported recently.[79] Since the strain-induced broken threefold symmetry shifts the valley magnetic moment at ±K points in momentum and the TRS dictates such shifts to be opposite in directions, the resultant Fermi pockets enclose different amounts of magnetic moment at the ±K valleys in the present of charge current, leading to a net magnetization.[80]

3.6. Spin-Valley Locking in Transition Metal Dichalcogenides

Remarkably, TMDs have strong spin–orbit coupling (SOC) that provides a unique system to study the coupling between spin and valley DoFs.[45] The strong SOC inheriting from the *d*-orbitals of the heavy metal atoms introduces a large split in the valence bands. According to first-principle calculations as well as experimental evidence, the SOC splitting energies are ≈150 meV in MoX_2 and ≈400 meV in WX_2, respectively.[17] Moreover, in 1L-TMDs, the mirror reflection symmetry about the metal atom plane only allows for spin oriented along the out-of-plane directions. Additionally, Additionally, as the K and −K valleys are related to each other by the time-reversal symmetry, the TRS requires that the spin splitting at different valleys should have identical magnitudes but opposite signs. These giant SOC energies along with the broken inversion symmetry give rise to a spin-valley locking effect that the spin index is locked to the valley index: valley K (−K) has only spin up (down) holes. The valley-contrast spin splitting can be probed by PL spectra—the A and B exciton emission peaks at different photon energies associated with two spin-splitting valence subbands, similar to the interband transitions involving heavy and light hole in III-IV semiconductors.[17,46] In this case, the optical selection rule is both valley- and spin-dependent, in other words, both the real spin and valley pseudospin can be selectively excited, as shown in **Figure 5**a.[17,46,83] Also, the intervalley scattering is largely suppressed because a simultaneous spin flip is required, thus both the valley and spin lifetimes are expected to be largely extended. Since the intervalley relaxation of spin and valley are slow, the generation of VHE may also engender a spin Hall effect.[45]

3.7. Spin-Layer Locking in Bilayer Transition Metal Dichalcogenides

In 2H-stacking bilayer TMDs, the SOC induced spin splitting has a sign dependence on both valley and layer indices, that is,

the Bloch states in ±K valley are strongly localized in either top or bottom layer depending on their spin orientation.[84] Because of the 2H-stacking order, the bottom layer is the 180° rotation of the upper layer; this rotation only switch two valleys in the bottom layer but leaves the spin unchanged. In other words, the spin splitting has opposite signs in a given valley that located in different layers (Figure 5b). This affords another degree of freedom called layer pseudospin, that is, an electronic state localized to the upper/bottom layer can be labeled with layer pseudospin up/down. Owing to the large SOC, both the intervalley and interlayer hopping are efficiently suppressed, leading to a spin-layer locking effect. Pseudospin up (down) corresponds to the state where the charge carrier is located in the upper (lower) layer, which leads to the electrical polarization of layer pseudospin. As a result, the spin-layer locking effect allows the manipulation of spins through gate control.[81,84] For example, a perpendicular electric field can lift the energy degeneracy between spin-up and -down states localized in opposite layers for a given valley, for example, the Zeeman splitting. The electrical modulation of this Zeeman splitting can be visualized from the magneto-transport measurements in WSe_2 (Figure 5c), where the magnetoresistance shows a crossover for weak localization to weak anti-localization with gate modulation.[82] Although possessing inversion symmetry, the exciton/trion emission in bilayer WX_2 (WSe_2 and WS_2) exhibits surprisingly robust circular dichroism ($|\eta| \approx \pm 95\%$ at 10 K), corroborating the strong interplay between the real spin and valley/layer pseudospins[46,81,85] (Figure 5d). In bilayer WSe_2, the trion emission peak splits into a doublet at large gate voltage, suggesting an electrically induced Zeeman splitting. Moreover, with negligible exchange interactions for interlayer trions, the consequent long-lived intervalley coherence leads to a strong linear polarization ($|\eta| \approx 80\%$).[81]

3.8. Valley Polarization Lifetime and van der Waals Heterostructures

The long valley polarization lifetime is essential for the realization of valleytronics devices for practical applications. In monolayer TMDs (1L-TMDs), the valley depolarization times were characterized by different methods, such as pump-probe measurements,[88] time-resolved PL,[89] Kerr,[90–92] and Faraday measurements,[93] and the measured neutral exciton polarization lifetimes were on the picosecond scale at low temperature (77 K or below). Experimental results indicate that the increase the energy and density of the excitation light and the sample temperature are responsible for the acceleration of the valley depolarization and thus leading to decreased valley polarization lifetimes in TMD monolayers.[65,66,68,91,94] So far, the electron-hole exchange interaction is believed to be the dominant depolarization mechanism for neutral excitons.[95,96] While for charged excitons, the electron-hole exchange is forbidden because of Pauli blocking, thus a much longer decay time (>1 ns) was observed, of which the depolarization mechanism was attributed to intervalley scattering.[89] Because the electron-hole exchange strength is proportional to their overlap probability, the interlayer excitons formed in the bilayer vdW heterostructure that are spatially separated are expected to have a longer lifetime.[97–102] With the all-dry transfer technique, 2D vdW heterostructure can be fabricated by stacking different 2D materials layer by layer.[103] **Figure 6**a shows a typical monolayer WSe_2–$MoSe_2$ vdW heterostructure.[86] Due to the large Coulomb interaction in 2D materials, and the prediction of staggered (type-II) band alignment between the proper pair of TMDs, the interlayer excitons/trions can be generated in heterostructures building from different types of 2D semiconducting TMDs, as illustrated in Figure 6b.[104–110] The depletion region is absent in these kinds of heterostructure due to the 2D nature, and the band offsets are large enough, thus ensuring a fast interlayer charge transfer for interlayer excitons formation (Figure 6c).[86,87,107,108,111] In 2016, Rivera et al. realized valley-specific interlayer excitons in monolayer WSe_2–$MoSe_2$ vertical heterostructure.[87] These interlayer excitons recombined radiatively and emit at an energy lower than $MoSe_2$ and WSe_2 exciton energy, resulting from the reduced bandgap shown in Figure 6c. Additionally, a valley lifetime of ≈40 ns was measured (gate voltage: 60 V), which is several orders of magnitude longer than that of the intralayer excitons in 1L-TMDs (Figure 6d). The reason for the much-extended lifetime lies in the separation of electron and hole in both real and momentum spaces. Under illumination, the photogenerated electrons and holes are confined in MoS_2 and WSe_2, respectively, hence the excitons are spatially-indirect, as shown in Figure 6e.[87,99] On the other hand, because of the lattice mismatch and the twisted angle between two individual layers caused in the stacking process, the ±K valleys are separated in momentum-space.[86] As a result, the valley scattering process is largely suppressed, leading to an extended valley polarization lifetime.

4. Quantum Hall Effect and Quantum Oscillations

Besides the quantum effects caused unique electron energy band structure and electronic polarization, the quantum effects of electron transport in 2DLMs (such as quantum Hall effects) are also of great importance. The quantum Hall effect (QHE), discovered in the 1980s, is one of the most remarkable phenomena in condensed matter physics, with its fundamental significance as a manifestation of quantum mechanics on a macroscopic scale.[112] QHE can only occur in 2D systems, for example, the 2D electron gases (2DEGs). When a 2DEG is subjected to a strong perpendicular B-field, the electron energy levels are quantized as discrete Landau levels (LLs). The Hall conductance σ_{xy} exhibits a plateau when the Fermi level E_F falls between LLs and a step when E_F crosses a LL. The QHE is always accompanied with the Shubnikov–de Haas (SdH) oscillations with the Hall plateau coincidental with the vanishing of longitudinal resistance σ_{xx}. The basic experimental characterization of QHE is the quantization of the Hall conductance

$$\sigma_{xy} = \frac{\nu e^2}{h}$$

and the nearly vanishing dissipation

$$\sigma_{xx} \to 0$$

of a 2D electron system subjected to strong perpendicular B-fields and low temperatures, where ν is the filling factor, e the

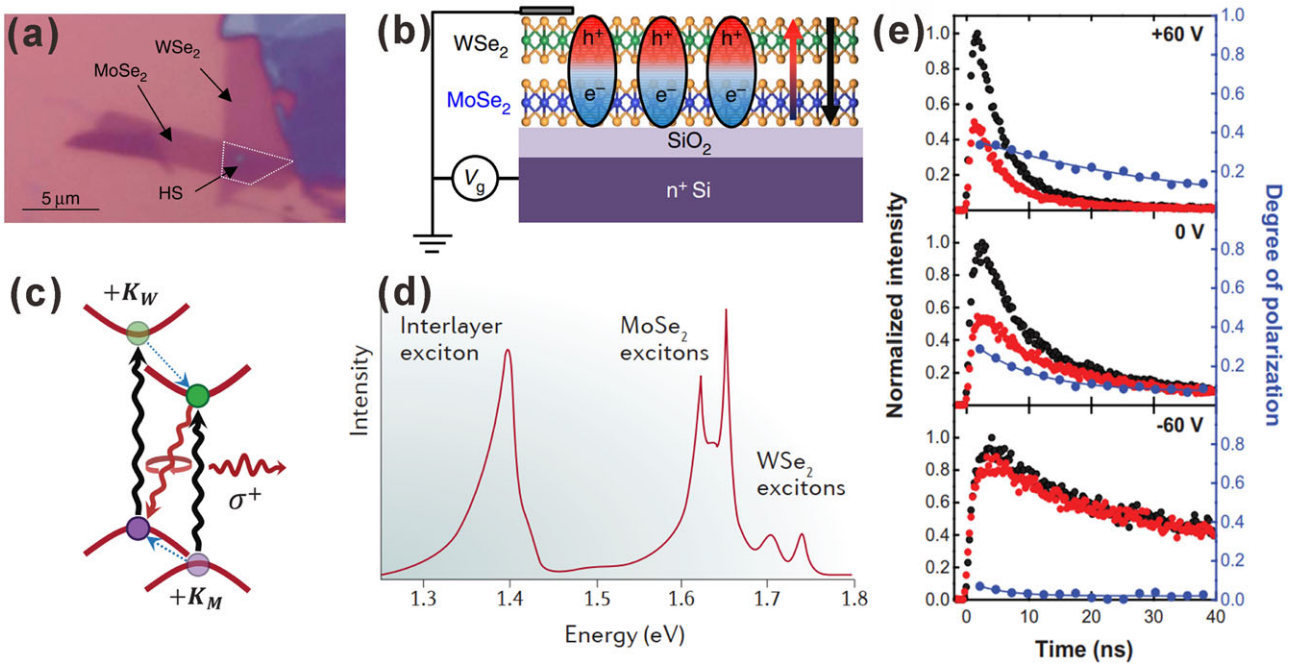

Figure 6. Interlayer valley excitons in MX_2–WX_2 heterostructures. a) Optical image of a typical monolayer WSe_2–$MoSe_2$ vertical heterostructure (HS). The white dash lines outline the HS region. Reprinted with permission.[86] Copyright 2015, Nature Publishing Group. b) Illustration of the spatially indirect, interlayer excitons in a WSe_2–$MoSe_2$ (X = S, Se) heterojunction device, with holes (h^+) and electrons (e^-) located in WSe_2 and $MoSe_2$, respectively. The red arrow shows the permanent dipole of the exciton pointing from $MoSe_2$ to WSe_2. The black arrow shows the applied electric field by a negative gate voltage V_g. Reprinted with permission.[86] Copyright 2015, Nature Publishing Group. c) Schematic of the exciton excitation/emission process in the +K valley. First, the σ^+ (right) circularly polarized light (black wavy lines) excites intralayer excitons in the $+K_M$ (+K valley of MoX_2) and $+K_W$ (+K valley of WX_2) valleys. Fast interlayer charge hopping (blue dotted lines) forms the interlayer exciton in the +K valley. The optical selection rules in the $+K_W$ and $+K_M$ valleys produce co-polarized PL. Reprinted with permission.[87] Copyright 2016, American Association for Advancement of Science. d) PL spectrum from a monolayer $MoSe_2$–WSe_2 heterojunction, indicating emission from both intralayer and interlayer excitons.[86] Reprinted with permission.[86] Copyright 2015, Nature Publishing Group. e) (Left axis) Time-resolved PL of interlayer excitons in the monolayer WSe_2–$MoSe_2$ heterojunction. (Right axis) The decay of valley polarization. Solid lines are single exponential fits to valley polarization decay, with lifetimes of ≈39, ≈10, and ≈5 ns for gate voltages of 60, 0, and −60 V, respectively. Reprinted with permission.[87] Copyright 2016, American Association for Advancement of Science.

elementary electron charge, and h the Planck constant. The dimensionless factor ν takes either an integer value (integer QHE, that is, IQHE) or a "simple" fraction p/q (fractional QHE, i.e., FQHE), with p and q being integer values. In the early studies of QHE, the 2DEGs were artificially constructed in a quantum well structure, such as the GaAs/AlAs heterostructure grown by molecular beam epitaxy (MBE) with extremely low disorder, and the QHE was observable only under low temperatures. With the emergence of graphene, which is a genuine 2D material and has exceptional high mobilities, the QHE can be observed in a much easier way.[3,112–115]

4.1. Quantum Hall Effect in Graphene

In 2005, the experimental observation of IQHE in graphene was first reported by Geim and Kim's group.[114,116] **Figure 7**a depicts the formation of LLs in graphene. These LLs consist of both an electron and a hole series of levels, in which the LL energy is expressed by

$$E_n = \mathrm{sgn}(n)\sqrt{2e\hbar v_F^2 |n| B}$$

Here $\hbar = h/2\pi$ is the reduced Planck's constant and the integer n represents an electron-like ($n>0$) or a hole-like ($n<0$) LL index. Crucially, an additional zero LL (zLL) $E_0 = 0$ is robust in graphene—regardless of the B-field—as long as the particle-hole symmetry is preserved.[114,116–118] As a result, the Hall conductance in graphene follows an unusual half-integer pattern

$$\sigma_{xy} = \pm 4\left(n + \frac{1}{2}\right)\frac{e^2}{h}$$

where the coefficient "4" comes from the fourfold degeneracy of LLs associated with spin and valley degeneracy; and the additional factor of "1/2" comes from the robust zLL at $n = 0$, which is in stark contrast to the conventional 2D systems with integer Hall plateaus.[117,118] Figure 7b shows a typical IQHE and the accompanied SdH oscillations in a SLG Hall-bar device. At high B-field (above 20 T), the zLL can split into two subbands at $\nu = \pm 1$ by lifting the sublattice degeneracy, suggesting a many-body effect related LL near the charge-neutral Dirac point.[119] As with many other quantum phenomena, the observation of QHE requires low temperature, typically below the liquid-helium temperatures.[113] One significance of graphene is that it extends the QHE temperature up to the unprecedented liquid-nitrogen temperature, or

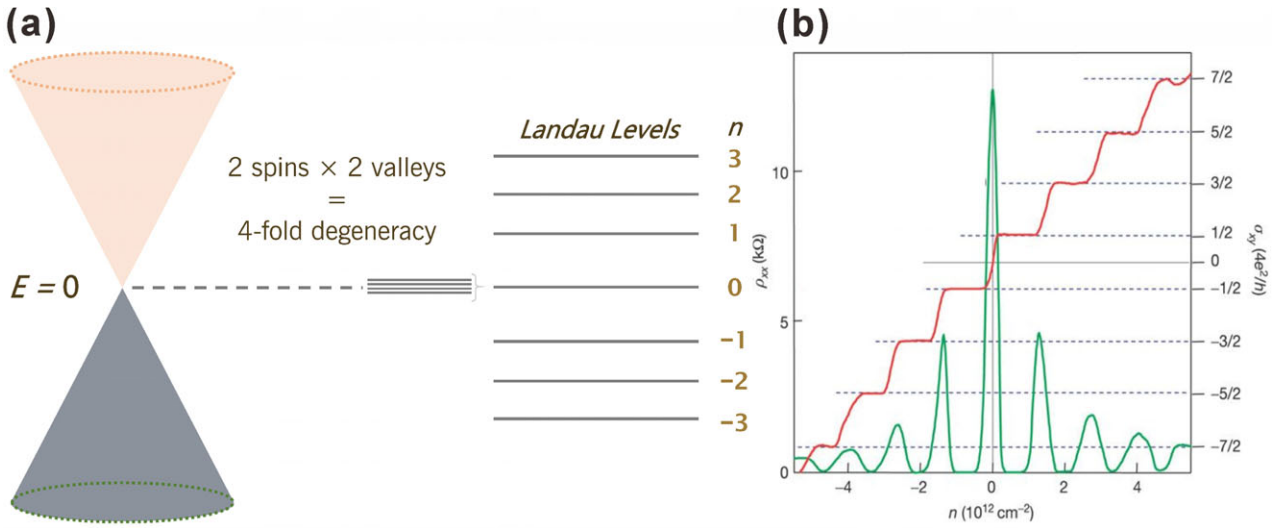

Figure 7. Quantum Hall effect in graphene. a) Schematic representation of the formation of Landau levels (LLs) in graphene (*n*: Landau index). The levels are not equally spaced and the positive/negative *n* values represent the electron/hole series of LLs. The zero LL at the neutral point ($E = 0$) has an associated LL. The LLs are four times degenerated because of the spin and valley pseudospin degrees of freedom. Reprinted with permission.[116] Copyright 2005, Nature Publishing Group. b) The integer Hall plateaus (σ_{xy}) and the SdH oscillations (ρ_{xy}) of graphene with tuned carrier density (n). The absence of plateau at $n = 0$ indicates the presence of a LL at the neutral point. Reprinted with permission.[116] Copyright 2005, Nature Publishing Group.

even room temperatures, due to the unusual charge carriers in graphene behaving as massless Dirac fermions and moving with ultrahigh mobilities.[3] As for FQHE, the experimental observation requires much more extreme conditions, such as the ultraclean sample, extremely low temperature and very strong *B*-field. Till now, the observation of FQHE has been demonstrated in suspended SLG,[120] BLG,[121–123] and TwBG,[124] but the underlying physical mechanism is rather intricate and beyond the scope of this review.

4.2. Quantum Spin Hall States in Graphene

The QSH system, also known as quantum spin Hall insulator (QSHI) or 2D topological insulator, has a charge exciton gap in the bulk, whereas the topologically protected gapless edge states reside in the bulk insulating gap.[126–129] The TRS endows these edge states with a unique helical feature: a pair of states with opposite spin polarization shall counterpropagate at a given edge, which is also known as the spin-momentum locking effect. The helical edge states are robust against non-magnetic disorders and the backscattering is strongly suppressed, provided that the TRS is preserved. The robust QHE electronic phases require a sufficient large and nontrivial gap in the 2D bulk, in the graphene case, the original Kane-Mele model proposes a SOC induced gap opening, however, it was shown to be unrealistic because the SOC in graphene is too weak and the gap is too small to support QSH states.[127,128] A possible solution is to find topological phases protected by symmetries other than TRS to realize QSH states in graphene. In SLG, the spin remains a good quantum number because of the weak SOC, and the electron and hole LLs near charge-neutral points are close enough to have band inversion caused by Zeeman effect, therefore a spin-symmetry-protected QSH phase is expected.[125] In the experimental demonstration, the *B*-field was tilted with respect to the graphene plane: the total *B*-field (B_T) was changed but the out-of-plane component ($B_\perp$) was fixed by varying the tilted angles. Since the orbital energies are exclusively coupled to $B_\perp$, while the spin-related Zeeman energy scales with B_T in regardless of the direction, the titled field scheme can quantitively extract the information about the net spin. At large B_T, the zLL is fully resolved into $\nu = 0, \pm 1$ plateaus;[119] specifically, the $\nu = 0$ state is spin-unpolarized and remains strongly insulting, whereas the $\nu = \pm 1$ states are conducive and spin-polarized due to the combined effects of Zeeman and QH ferromagnetism.[118,130,131] The combined capacitance and conductance measurements showed that, as the B_T became large enough (35 T) with $B_\perp$ held constant at 1.5 T, the SLG entered in to in the QSH regime: the edge gap closing occurred whilst the $\nu = 0$ insulting bulk sustained, giving rise to an incompressible bulk gap and robust conducting edge states (**Figure 8**a,b). For BLG, the QSH state can be realized with the $\nu = 0$ state.[132–136] Maher et al. utilized top and bottom gates to independently control the carrier density and perpendicular electric displacement field *D* in BLG, as well as a tilted *B*-field to adjust the Coulomb energy and Zeeman energy separately. At finite *D* and large in-plane *B*-field ($B_T \gg B_\perp$), a level crossing occurs at the edge and thus developing spin-polarized counter-propagating edge states, manifesting as a metallic four-terminal conductance of $\approx 4e^2/h$.[132] However, the implementation of such QSH phases in SLG/BLG suffers from the disadvantage of the requirement of large *B*-fields exceeding 20 T because of the relatively weak Zeeman coupling in this system, which is not easily accessible in common laboratories. Sanchez-Yamagishi et al. developed a decoupled graphene electron-hole bilayer system to realize the QSH states at much weaker *B*-fields (Figure 8c).[124] In this scheme, firstly, two SLG were stacked with a twisted misalignment to cause a low-energy decoupling in these two layers

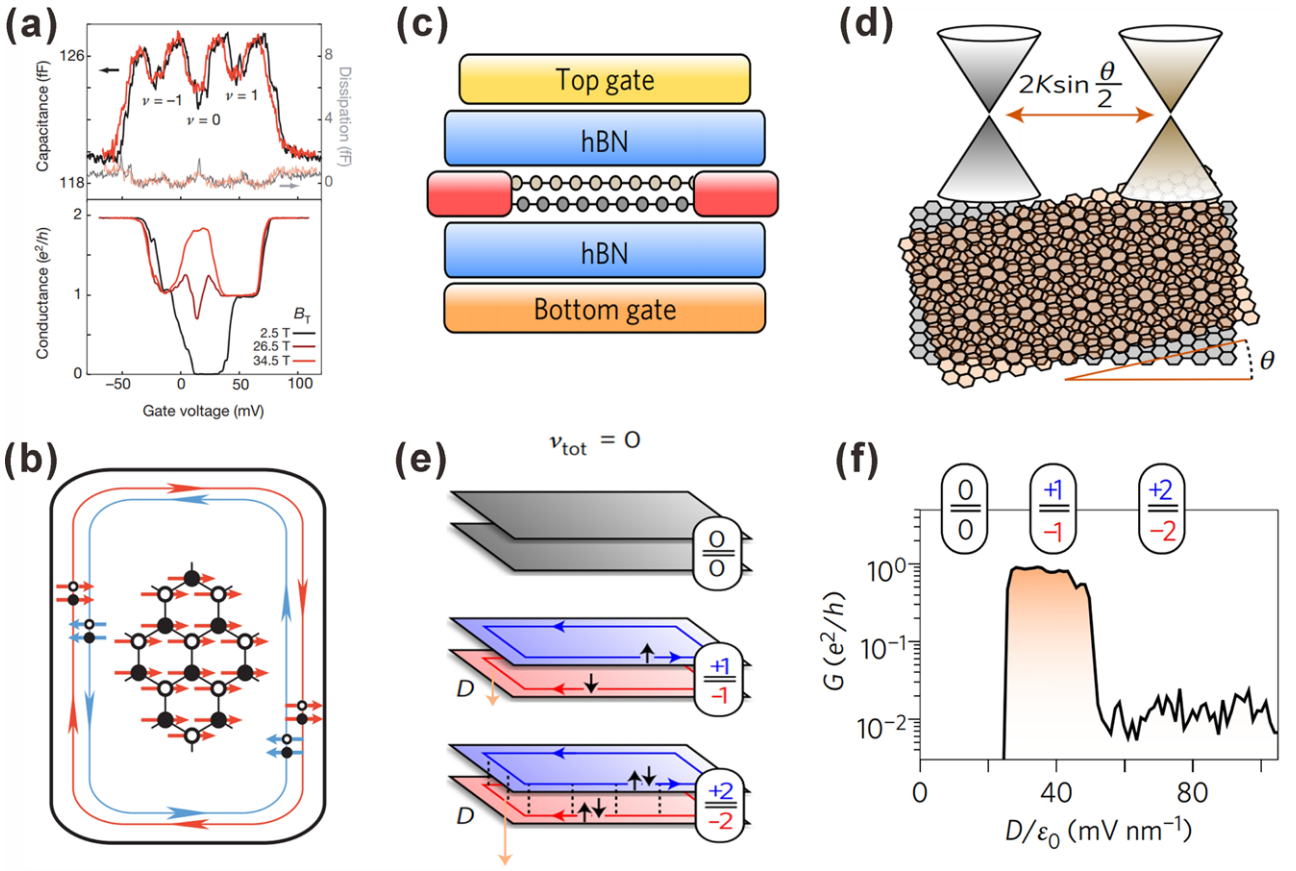

Figure 8. Quantum spin Hall (QSH) effect in graphene. a,b) QSH states in monolayer graphene under tilted magnetic fields ($B_\perp = 1.4$ T for different B_T). Reprinted with permission.[125] Copyright 2014, Nature Publishing Group. a) (Top) Capacitance and dissipation and (Bottom) conductance at $B_\perp = 2.5$ T for a monolayer graphene device. The dips of capacitance represent the quantized hall states within the zero Landau level at $\upsilon = 0$ and ± 1.The low dissipation confirms the low-frequecy limit. As at B_T is increased, the conductance undergoes a transition from an insulating ($B_T = 2.5$ T) to a metallic state ($B_T = 34.5$ T), accompanied with the undetectable change in capacitance, indicating that such transition is due to the emergence of gapless edge states with an incompressible bulk. b) Schematic diagram of the spin configuration of bulk and edge states in monolayer graphene when entering into the fully polarized QSH regime. Arrows show the projection of the electron spin on a particular sublattice with the two sublattices marked by open and filled circles. c–f) QSH states in twisted bilayer graphene (TwBG) under moderate *B*-fields. Reprinted with permission.[124] Copyright 2017, Nature Publishing Group. c) Device structure of TwBG encapsulated in *h*BN with dual-gates scheme. The red boxes indicate the contact electrodes. d) Schematic diagram of the stacked two graphene layers with a relative twisted angle θ which decouples the Dirac cones from each layer via a large momentum mismatch ($K = 4\pi/3a$, a: graphene lattice constant). e) Schematic diagram of the edge-state configurations with zero total filling factor ($\upsilon_{tot} = 0$). Black arrows indicate the spin direction and the red/blue arrows show the electron/hole-like chirality. f) Conductance for $\upsilon_{tot} = 0$ of the TwBG device as a function of electric displacement field, *D*, at $B = 4$ T. The $(-1, +1)$ state is conductive while the $(-2, +2)$ state is insulating.

(Figure 8d). Then, the top and bottom layers are controlled by a dual-gate structure with one layer being tuned into hole-doped regime while the other layer into electron-doped regime. Under a moderate *B*-field (4 T), the weak interlayer coupling allows the independent development of gapless edge states with opposite chiralities and opposite filling factors $\nu = \pm 1$; accompanied with the strongly suppressed backscattering, a highly conductive 1D transport edge with conductance ranging from 0.8 to 1.5 e^2/h was achieved in such twisted bilayer graphene (TwBG) QSH system (Figure 8e,f). Unlike the case in the aforementioned QSH states in SLG, where the spin polarization in edge states stem from Zeeman coupling, the electronic interactions are the key factors to the implementation of QSH phases in the TwBG.[137] Recently, Stepanov et al. reported a robust spin transport in charge-neutral graphene by utilizing the $\nu = 0$ state as the antiferromagnetic insulator and combining the $\nu = \pm 2$ and $\nu = \pm 1$ states to implement spin injectors and detectors with a long non-local transport distance up to 5 µm.[138]

4.3. Observation of Quantum Transport in 2D Layered Materials Beyond Graphene

In the mostly studied 2DLMs other than graphene, such as TMDs, InSe, and BP, the exploration of quantum transport becomes even more arduous due to the moderate carrier mobilities, typically—if without special treatment—at the order of 0.1 to 100 $m^2\ s^{-1}$ for 1L-TMDs and ≈1000 $m^2\ s^{-1}$ for multilayer BP at room temperature, and these values become even smaller at low temperatures.[143–145] One the other hand, sufficiently high carrier mobility at low temperatures is an essential factor to observe

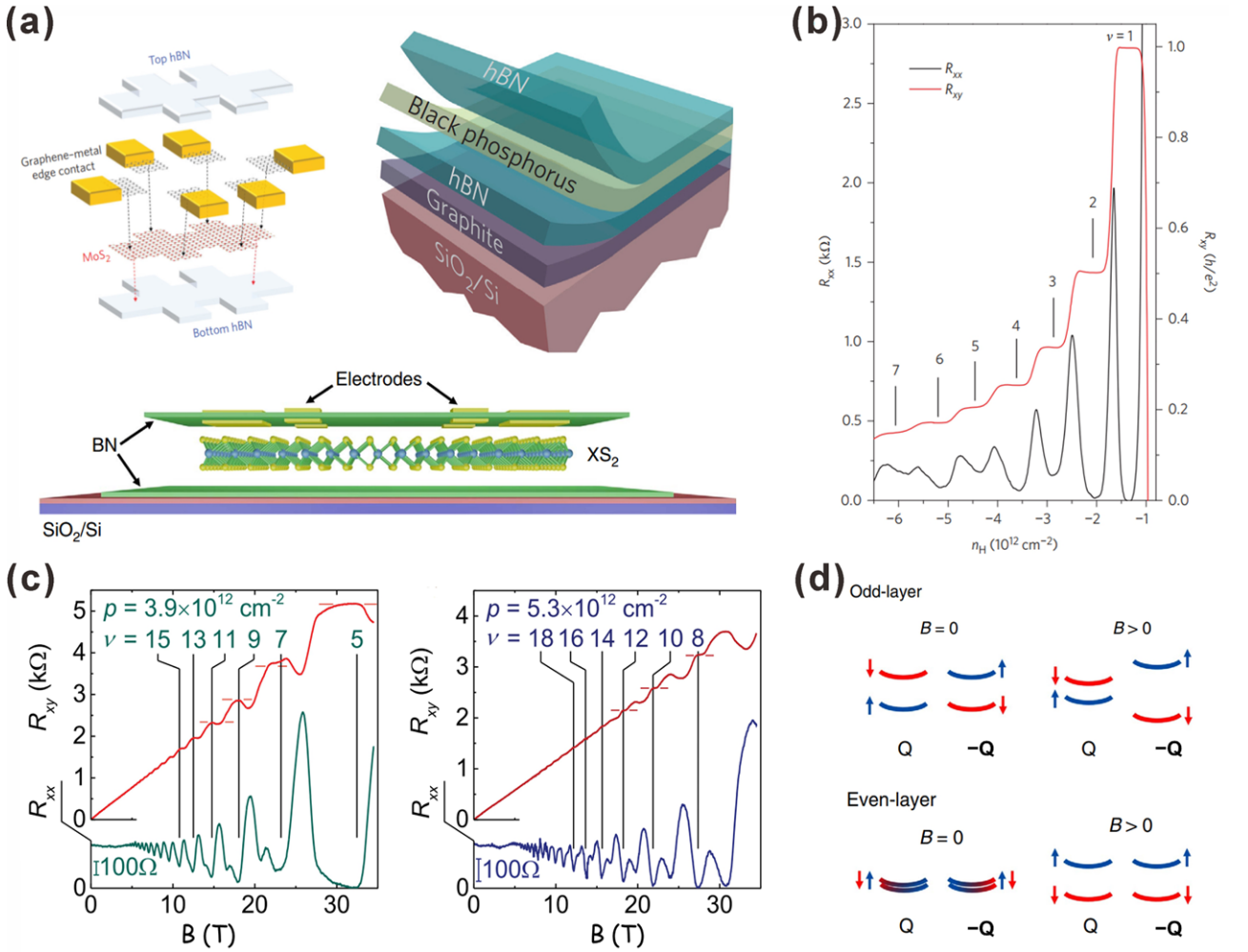

Figure 9. Quantum Hall effects in BP and TMDs. a) Some typical device structures for achieveing high carrier mobility and low contact resistance in BP and TMDs. Reprinted with permission.[139–141] Copyright 2015 and 2016, Nature Publishing Group. b) Quantum Hall plateaus (R_{xy}) and SdH oscillations (R_{xx}) as a function of carrier density (n_H) in a few-layer BP device. The minus sign of n_H means BP is in hole-doped regime. The integers indicate the quantum Hall state with filling factor υ from 1 to 7, indicating the degeneracy of LLs in BP is fully lifted. Reprinted with permission.[140] Copyright 2016, Nature Publishing Group. c) Quantum Hall plateaus (R_{xy}) and SdH oscillations (R_{xx}) as a function of magnetic field in a bilayer WSe_2 device at different p-doping level: (left) $p = 3.9 \times 10^{12}$ cm^{-2} showing quantum Hall states at predominantly odd filling factors and (right) 5.3×10^{12} cm^{-2}, showing quantum Hall states at predominantly even filling factors. Reprinted with permission.[142] Copyright 2017, American Physical Society. d) Schematic diagrams showing the valley Zeeman splitting and spin Zeeman splitting at $\pm$Q valleys in odd- and even-layer MoS_2 devices, respectively. For odd-layer MoS_2, the sub-band at Fermi level is non-degenerate at $B = 0$; at $B > 0$, the degeneracy between Q and $-$Q valleys is lifted by the valley Zeeman effect. For even-layer MoS_2, the sub-band at Fermi level is spin-degenerate at $B = 0$; at $B > 0$, the degeneracy between spin-up and spin-down states at $\pm$Q valleys is lifted by the spin Zeeman effect. Reprinted with permission.[141] Copyright 2016, Nature Publishing Group.

the quantum mechanics enhanced transport phenomena, for example, the onset B-field for observing SdH oscillations is normally the reciprocal of carrier mobility (in the unit of m^2 s^{-1}).[146] Therefore, with the B-field that can be achieved in current laboratory conditions, the SdH oscillations in these 2DLMs are not observable, not to mention the QHE. Such moderate mobilities are limited by disorders, intrinsic defects, interfacial charge traps, etc., and scientists have come up with several solutions to improve the carrier mobilities, such as dielectric screening,[147,148] chemical doping,[149,150] and hBN encapsulation.[139,151,152] **Figure 9**a introduces several typical device schemes for achieving high carrier mobilities and low contact resistance in 2D materials with the sandwiched heterostructure. By encapsulating 2DLMs between hBN layers, the interfacial scattering from substrate phonons and charge traps are reduced, and the screening from surface adsorbates can be increased, thereby largely enhancing the carrier mobility of 2DLMs.[139,151] In MoS_2, via combining the hBN encapsulation with the graphene contacts, which can effectively reduce the contact resistance down to 100 Ω µm, the low-temperature mobilities reach the highest measured values to date: ≈34 000 cm^2 V^{-1} s^{-1} for 6-layer MoS_2 and ≈1020 cm^2 V^{-1} s^{-1} for 1L-MoS_2.[139] For few-layer BP, the hBN/BP/hBN sandwiched structure gives rise to the record-breaking hole mobility of ≈5200 cm^2 V^{-1} s^{-1} at room temperature and ≈45 000 cm^2 V^{-1} s^{-1} at low temperatures.[153] With such largely enhanced low-temperature mobilities, the

experimental observations of both SdH oscillations and QHE at realistic B-field are possible in such materials.

The effective Landé g factor g^* and effective mass m^* of carriers are two crucial parameters charactering the energy gap of LLs. In 2DEGs, the observed QH states sequence always reflect the energy ratio between the Zeeman energy $E_z = g^*\mu_B B$ and cyclotron energy $E_c = \hbar\omega_c$, here μ_B is the Bohr magneton and ω_c is the cyclotron frequency. Normally, the Zeeman energy E_z scales with the total field B_T, while the cyclotron energy E_c depends solely on the $B_\perp$ ($\omega_c = eB_\perp/m^*$), and the resultant ratio E_z/E_c can be expressed as:

$$\frac{E_z}{E_c} = \frac{g^*\mu_B B}{\hbar\omega_c} = \frac{g^* m^*}{2m_0}\cos\theta, \left(\mu_B = \frac{e\hbar}{m_0}\right),$$

where θ is the tilting angle between the B_T and the perpendicular direction ($B_\perp = B_T cos\theta$), and m_0 is the free electron mass, respectively. Therefore, by tuning the tilting angle θ, the resultant LL crossings at certain values of θ provide a standard method to determine the ratio E_z/E_c and the spin susceptibility $\chi = g^*\mu_B B/2\pi\hbar^2 \propto g^* m^*$. In the standard measurements, the effective mass m^* can be extracted from the SdH measurements, in which the temperature-induced damping of the longitudinal resistance R_T follows the formula $R_T = \xi/\sinh(\xi)$, $\xi = 2\pi^2 k_B T/\hbar\omega_c$ (k_B: Boltzmann constant). Therefore, g^* can be determined from the measured χ and m^*.[154]

4.4. Quantum Transport in Black Phosphorus

In the p-type BP, the quantum transport measurements are always carried out in the hBN/BP heterostructure or hBN/BP/hBN encapsulation system.[140,155–157] With local back gate tuning, Li et al. unraveled the 2D nature of the negative gated BP thin flakes with holes are confined in a 2-nm quantum well (≈2 atomic layer) along the out-of-plane direction.[140] Such BP 2D system, together with the exceptional high carrier mobility and the flexible tunability of the type of charge carriers, enable the observation of QHE in both electron and hole doped regime (Figure 9b).[140,155] Unlike the fourfold degeneracy in graphene, the LLs in BP are twofold degenerate and can be fully lifted at large B-fields, which manifests as the QH states revealed at both even and odd filling factors υ. The effective g-factor can be characterized by means of the tilted-field and temperature-dependent measurements. Long et al. reported a large g^* value of ≈2.8 enhanced by the exchange interactions between spins in opposite directions,[155] while Li et al. reported a g^* value of ≈2 for $\upsilon = 5$ to 15, which, however suggesting a negligible enhancement.[140]

4.5. Quantum Transport in Transition Metal Dichalcogenides and Semimetal Chalcogenide

The QH plateaux sequence measured in the 2D WSe_2 shows a twofold degeneracy and is insensitive to the in-plane component of the B-field.[142,158] This arises from the large SOC induced extremely large splitting energy (≈640 meV in 1L-WSe_2 and ≈80 meV in 2L-WSe_2) and the mirror symmetry, whereby the hole spin is locked to the out-of-plane direction and therefore only responds to the $B_\perp$.[142,159,160] Moreover, Figure 9c shows a density-dependent QH plateaus sequence in bilayer WSe_2, and such sequence is controlled by the E_z/E_c ratio. Specifically, as E_z/E_c close to an even/odd integer, the filling factors are predominantly odd/even. The g^* value is largely enhanced with reduced carrier density due to the strong electron-electron interactions.[142] For multilayer WSe_2, Xu et al. observed an unconventional QH states sequence with predominantly odd-integer filling factors at moderate B-fields.[161] The SdH and QHE measurements unraveled a giant spin susceptibility $\chi \approx 5.65m_0$ and a large hole mass of $m^* \approx 0.8m_0$ in 8-layer WSe_2, giving rise to an extremely large $g^* \approx 6.52$. These large values of g^* are closely correlated to the thickness dependent band structure of WSe_2. Unlike the 1L(2L)-WSe_2 where the VBMs are located at ±K points, the multi-layered counterparts are located at the Γ point. Therefore, the QH transport in 1L(2L)-WSe_2 and multilayer WSe_2 are dominated by K-valley holes and Γ-valley holes, respectively. However, unlike those orbitals at ±K points with strong SOC, the orbitals at Γ point are composed of the delocalized out-of-plane $5d_{z^2}$ orbitals of W atoms, thereby a negligibly weak SOC. As a result, the enhanced g^* in 8-layer WSe_2 is reasonably attributed to the short-range electron-electron interactions, rather than the SOC in mono- and bilayer cases.[161]

Different from the p-type WSe_2, the QH transport in the n-type MoS_2 and WS_2 is dominated by the Q-valley electrons, for the reason that the CBM states in multilayer Mo/WS_2 are not located at ±K points, but rather at ±Q points.[141,162,163] Related by the threefold rotational symmetry, these six Q valleys consist of three ±Q pairs. As shown in Figure 9d, for the even-layer, each pair of ±Q valley is further related by spatial inversion symmetry and TRS, which requires Kramers degeneracy. Consequently, the SdH oscillations in even-layer MoS_2 exhibit a 12-fold degeneracy at low fields and sixfold degeneracy at high fields because of spin Zeeman splitting within each valley. While for the odd-layer, due to the broken inversion symmetry, the spin degeneracy at each Q valley is already lifted at $B = 0$. Therefore, the QH transports in odd-layer MoS_2 are significantly different. In odd-layer MoS_2, the SdH oscillations show sixfold LL degeneracy at low fields and reduce to a threefold one at high fields due to the valley Zeeman effect, much analogous to that in ±K valleys.[141]

WTe_2, another member in the TMD family, however, is a semimetal with high low-temperature mobilities. Unlike the abovementioned semiconducting TMDs, the SdH oscillations indicated the 3D feature of WTe_2 even in its few-layer forms.[22,23] On the other hand, when down to monolayer, the non-local electrical transport measurements implied that, at low temperature (<100 K), monolayer WTe_2 becomes insulating in its interior, while the edges remain conducting.[25] There are several circumstantial experimental evidences which suggest that monolayer WTe_2 possesses a helical edge mode, rather than a trivial edge mode: 1) the edge conductance is roughly independent of gate voltage; 2) the edge conducting is absent in bilayer due to the allowed backscattering between top and bottom layers; 3) the edge conductance in monolayer is largely suppressed by $B_{//}$, as the backscattering is allowed once the TRS is broken. Such nontrivial helical edge states are consistent with the theoretical predication that the Weyl semimetal WTe_2 being a 2D TI if a bulk gap opens.[164] Nevertheless, more solid experimental results, such as

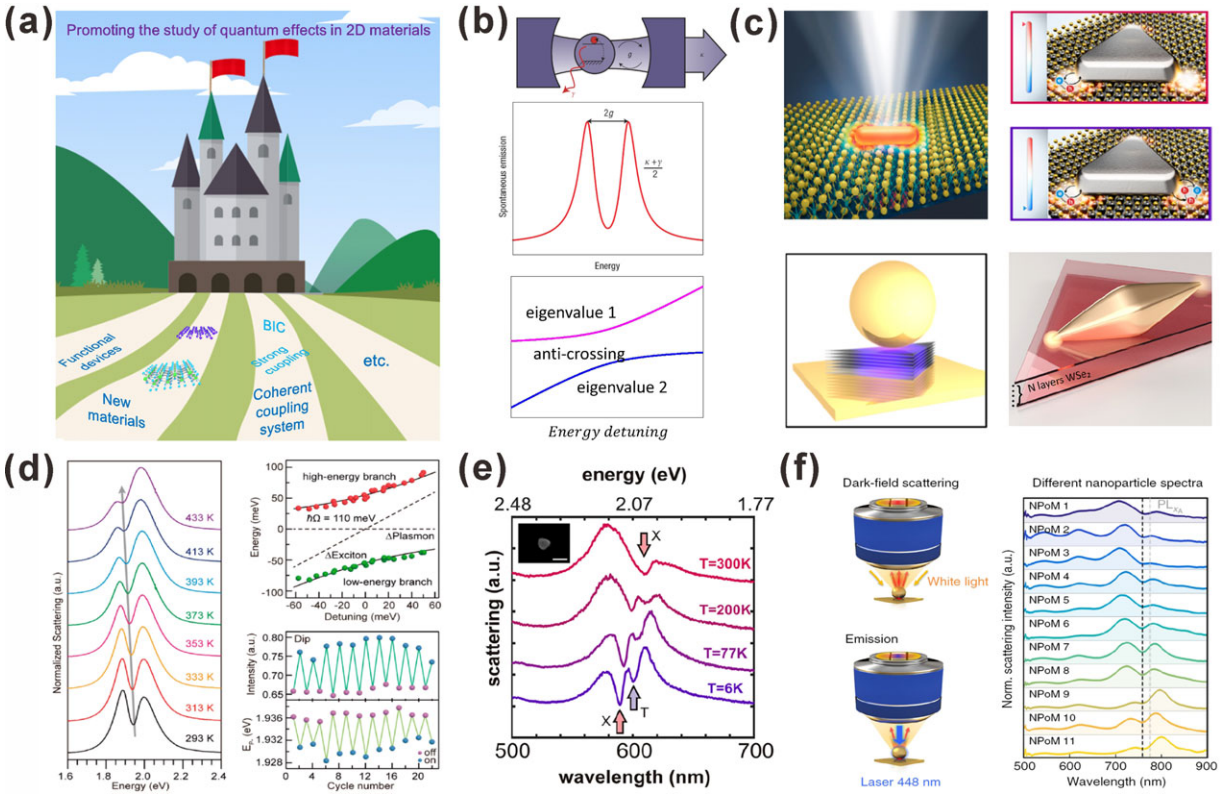

Figure 10. The outlook of studying quantum effects in 2D material systems. a) The study of quantum effets in 2D material systems are expected to be promoted by three main routes, which are exploring new materials, developing novel fucntional devices, and investigating new systems such as the coherent coupled system involevd 2D materials. b,c) The introduction of representive works about studying conherent coupling (i.e., strong coupling) between the exctions of 2D materials and plasmonic nanocavities. b) The condition for constructing a strong coupling system. Reprinted with permission.[195] Copyright 2006, Nature Publishing Group. c) Typical strong couplings involve 2DLMs. Reprinted with permission.[203–206] Copyright 2017, American Chemical Society; Copyright 2018, American Chemical Society; Copyright 2017, Nature Publishing Group; Copyright 2018, American Chemical Society. d) Dynamic tuning of strong coupling via temperature and electrostatic grating enabled by the 2DLMs. Reprinted with permission.[203] Copyright 2017, American Chemical Society. e) The formation of three bright intermixed plasmon-exciton-trion polariton states in the WS_2 involved strong coupling system. Reprinted with permission.[204] Copyright 2018, American Chemical Society. f) Studying the influence of dipole orientation on strong coupling. Reprinted with permission.[205] Copyright 2017, Nature Publishing Group.

the quantized conductance plateaux, are still needed to support this conclusion.

Recently, another layered 2D semiconductor InSe, was shown to possess high carrier mobilities of 10^3 $cm^2V^{-1}s^{-1}$ and 10^4 $cm^2V^{-1}s^{-1}$ at room and liquid-helium temperatures, respectively, which afforded the observation of fully developed SdH oscillations and QHE in multilayer films (>3L). For 6L InSe measured at 30 T and 2.5 K, the QH plateaus revealed LLs at all odd and even filling factors $1 \leq \upsilon \leq 10$, indicating a lifted spin degeneracy.[13] However, the SdH oscillations and QHE were not able to be measured in 1L-InSe, possibly due to the large contact resistance or the easy degradation of such ultimately thin films.[13]

5. Outlook and Discussion

The abundant members in the 2D layered materials family afford versatile opportunities and open innovative perspectives for exploring fundamental science and nanodevice applications covering the fields of electronics, photonics, optoelectronics, spintronics, and valleytronics.[41,48,58,143,165–169] In this review, we summarized the impressive quantum effects recently discovered in representative 2DLMs, which are caused by quantum behaviors of the 2D electrons from three main perspectives, that is, the evolution of electronic band structure, electronic polarization, and electronic transport. Although these quantum effects are introduced in succession, they can actually coexist in a same 2DLM system.[170–172] Moving forward, we anticipate more in-depth understanding of quantum effects in 2DLMs, and the new discoveries may be stimulated from three general aspects (**Figure 10**a).

First, with the devotion of substantial research efforts, a number of new 2DLMs can be explored, with notable discoveries benefiting both fundamental and applied studies of quantum science. For example, the emergence of 2D magnetic insulators (e.g., CrI_3) extends the possibilities of novel device applications,[173–176] such as spin-filters and valley manipulation, through vdW heterostructure engineering.[77,177,178] Besides, similar emerging 2DLM systems of VSe_2, $VAgP_2S_6$, $CuCrP_2S_6$, and $MnPSe_3$ have also aroused much attention due to their outstanding performances in building ferrovalley devices and spin electronics.[179–182]

Second, based on these fundamental discoveries of the quantum effects, together with the developments of nanotechnologies, a large variety of advanced functional quantum devices can be realized. For 2D semiconductors, the various and feasibly tunable energy bandgaps ranging from visible light to mid-IR are readily suitable for the optoelectronic applications, such as photodetectors and light emitters.[41,48] Also, benefiting from the free of dangling bonds in 2DLMs, it is both intriguing and realistic to construct functional vdW heterostructures without the constraints of lattice matching, in which the desirable advantage of each material can be leveraged. For example, the graphene/TMD/graphene can combine the ultrafast photoresponse of graphene and the large optical absorption of TMD to build high-speed and broadband photodetectors with high efficiency and photoconductive gain.[183–185] Another example is the stacking of intrinsically p-type and n-type 2D semiconductors to realize devices in the p-n diode fashion.[104,111,186–188] More complexly, the flexible quantum-well structure created by stacking graphene electrodes and repeated structure of sandwiched semiconducting 1L-TMDs between insulating *h*BN can minimize the leakage current to promise an efficient electron-to-photon conversion, leading to a high quantum efficiency of ≈10%, which is comparable to those organic LEDs and quantum-dot LEDs.[189,190] The valley-contrasting optical selection rule in TMDs can be utilized to build optoelectronics with valley functionalities. In a valley light emitting diode (LED) which converts electrical signal into polarized emission light, the valley-polarized electrons and holes can be electrically injected and the consequent EL emission exhibits an overall polarization. The EL polarization can be effectively moderated by the gate voltage or the magnitude of injection current.[70–72] By utilizing the spin-valley locking effect, the helicity of the emitted light can also be controlled through the injection of spin-polarized holes via a diluted ferromagnetic semiconductor, such as (Ga,Mn)As.[191] The complementary effect of valley EL is the conversion of circularly polarized light information into valley-dependent photocurrent. In such a photodetection device, the generation of valley-dependent photocurrent can be moderated by the handedness of the illumination light and the electrical detection can be realized by a lateral spin-valve structure using ferromagnetic contacts.[192,193]

Moreover, beyond the possibility of investigating quantum effects resulted from the electrons of 2DLMs, another emerging field of interest is to explore quantum phenomena in the coherent coupling systems involved 2D materials, which not only brings about new fascinating findings on quantum effects (such as Rabi splitting or Rabi oscillations), but also provides possibilities for expanding our understanding in quantum science for various applications . For example, according to the theory of cavity quantum electrodynamics (CQED), when the coupling strength between a quantum emitter and a cavity is greater than both the decays of emitter and cavity, the system reaches strong coupling region, characterizing as Rabi splitting and Rabi oscillation in the frequency and time domain, respectively (Figure 10b).[194,195] The strong coupling system is a typical coherent coupling system which can sustain coherent states with long de-coherent time that allows advanced quantum technologies such as constructing quantum network and controllable quantum manipulations, greatly benefiting quantum communication and computing.[194–200] Constructing a strong coupling system requires the quantum emitter with large transition momentum, which perfectly matches the advantage of strong excitonic effect in 2DLMs.[201,202] Therefore, with the employment of 2DLMs, numbers of investigations with novel observations in the field of strong coupling are performed.[203–215] Figure 10c illustrates the representative strong coupling systems constructed by 2DLMs and plasmonic nanocavities, where the TMDs together with a single plasmonic nanostructure or the nanoparticle on nanofilm structure are chosen.[203–206] Except for the advantage of large dipole momentum, the 2DLMs also exhibit the merit of controllable excitonic transition energy via the approaches of electrostatic grating, thermal scanning, or optical pumping. So, comparing with strong coupling systems with other quantum emitters, the 2DLM strong coupling system can offer the opportunities for strong coupling manipulation in facile and controllable ways (Figure 10d).[203,212,213] Moreover, the abundant physical properties of the excitons in 2DLMs also bring about plenty of novel discoveries. For instance, as shown in Figure 10e, a stable trion state can exist in the WS_2 system at low temperature, which enables the forming of three bright intermixed plasmon-exciton-trion polariton states.[204] Also, as the dipole orientation of 2DLMs can be modulated by changing the layer number, the 2DLM system provides an ideal platform for studying the dipole orientation dependence on strong coupling in experiments (Figure 10f).[205] Despite the plasmonic nanocavities, the 2D materials with outstanding performances of being quantum emitters can also be coupled to other nanostructures such as photonic crystal cavities and metasurfaces, as well as the optical bound states in the continuum (BIC).[216–223] Such coupled systems enable the investigations of nano-lasing, photon blockade, and single photon emitting, which affords innovative device architectures and novel research perspectives in the realm of quantum physics. With continuous efforts devoted, we envision the combining research from the perspective of both the fundamental science and technological applications, and on both the individual and coupled systems, to more profoundly investigate the quantum effects in 2DLMs, thus leading to greater achievements for quantum science and technology.

Acknowledgements

This work was supported in part by the National Key R&D Program of China (2016YFA0301300), the Shenzhen Science and Technology Research Funding (JCYJ20180507182429941), the National Natural Science Foundation of China (61675237), the Guangdong Natural Science Funds for Distinguished Young Scholars (2017B030306007), the Guangdong Special Support Program (2017TQ04C487), the Pearl River S&T Nova Program of Guangzhou (201806010033), the Guangdong Natural Science Foundation (2016A030312012), the Science and Technology Projects of Guangzhou (201607020023, 201805010004, and 201804010175), the Guangdong Province Public Interest Research and Capacity Building Special Fund (2017A020216020), and the Leading Talents of Guangdong Province Program (00201520). In addition, the authors thank Dr. Jiahong Wang, Dr. Ying Yu, Limin Lin, Wenbo Zhang, and Chao Guo for helpful discussions.

Conflict of Interest

The authors declare no conflict of interest.

Keywords

2D layered materials, quantum confinement, quantum effects, quantum Hall effects, valleytronics

Received: December 29, 2018
Revised: April 20, 2019
Published online: May 14, 2019

[1] C. Tan, X. Cao, X.-J. Wu, Q. He, J. Yang, X. Zhang, J. Chen, W. Zhao, S. Han, G.-H. Nam, *Chem. Rev.* **2017**, *117*, 6225.
[2] K. S. Novoselov, A. K. Geim, S. V. Morozov, D. Jiang, Y. Zhang, S. V. Dubonos, I. V. Grigorieva, A. A. Firsov, *Science* **2004**, *306*, 666.
[3] K. S. Novoselov, Z. Jiang, Y. Zhang, S. Morozov, H. L. Stormer, U. Zeitler, J. Maan, G. Boebinger, P. Kim, A. K. Geim, *Science* **2007**, *315*, 1379.
[4] K. F. Mak, K. He, C. Lee, G. H. Lee, J. Hone, J. Shan, T. F. Heinz, J. Shan, *Nat. Mater.* **2013**, *12*, 207.
[5] X. Ling, H. Wang, S. Huang, F. Xia, M. S. Dresselhaus, *Proc. Natl. Acad. Sci. USA* **2015**, *112*, 4523.
[6] D. R. Cooper, B. D'Anjou, N. Ghattamaneni, B. Harack, M. Hilke, A. Horth, N. Majlis, M. Massicotte, L. Vandsburger, E. Whiteway, *ISRN Condens. Matter Phys.* **2012**, *2012*, 1.
[7] J. R. Schaibley, H. Yu, G. Clark, P. Rivera, J. S. Ross, K. L. Seyler, W. Yao, X. Xu, *Nat. Rev. Mater.* **2016**, *1*, 16055.
[8] K. F. Mak, C. Lee, J. Hone, J. Shan, T. F. Heinz, *Phys. Rev. Lett.* **2010**, *105*, 136805.
[9] I. G. Lezama, A. Arora, A. Ubaldini, C. Barreteau, E. Giannini, M. Potemski, A. F. Morpurgo, *Nano Lett.* **2015**, *15*, 2336.
[10] Q. H. Wang, K. Kalantar-Zadeh, A. Kis, J. N. Coleman, M. S. Strano, *Nat. Nanotechnol.* **2012**, *7*, 699.
[11] A. Splendiani, L. Sun, Y. Zhang, T. Li, J. Kim, C.-Y. Chim, G. Galli, F. Wang, *Nano Lett.* **2010**, *10*, 1271.
[12] P. Miró, M. Ghorbani-Asl, T. Heine, *Angew. Chem. Int. Ed.* **2014**, *53*, 3015.
[13] D. A. Bandurin, A. V. Tyurnina, L. Y. Geliang, A. Mishchenko, V. Zólyomi, S. V. Morozov, R. K. Kumar, R. V. Gorbachev, Z. R. Kudrynskyi, S. Pezzini, *Nat. Nanotechnol.* **2017**, *12*, 223.
[14] J. F. Sanchez-Royo, G. Munoz-Matutano, M. Brotons-Gisbert, J. P. Martinez-Pastor, A. Segura, A. Cantarero, R. Mata, J. Canet-Ferrer, G. Tobias, E. Canadell, J. Marques-Hueso, B. D. Gerardot, *Nano Res.* **2014**, *7*, 1556.
[15] A. Kuc, N. Zibouche, T. Heine, *Phys. Rev. B* **2011**, *83*, 245213.
[16] C. Ruppert, O. B. Aslan, T. F. Heinz, *Nano Lett.* **2014**, *14*, 6231.
[17] H. Zeng, G. B. Liu, J. Dai, Y. Yan, B. Zhu, R. He, L. Xie, S. Xu, X. Chen, W. Yao, X. Cui, *Sci. Rep.* **2013**, *3*, 1608.
[18] Y. Wu, D. Mou, N. H. Jo, K. Sun, L. Huang, S. Bud'Ko, P. Canfield, A. Kaminski, *Phys. Rev. B* **2016**, *94*, 121113.
[19] Z. Zhu, X. Lin, J. Liu, B. Fauqué, Q. Tao, C. Yang, Y. Shi, K. Behnia, *Phys. Rev. Lett.* **2015**, *114*, 176601.
[20] Y. Yi, C. Wu, H. Wang, H. Liu, H. Li, H. Zhang, H. He, J. Wang, *Solid State Commun.* **2017**, *260*, 45.
[21] I. Pletikosić, M. N. Ali, A. Fedorov, R. Cava, T. Valla, *Phys. Rev. Lett.* **2014**, *113*, 216601.
[22] L. Wang, I. Gutiérrez-Lezama, C. Barreteau, N. Ubrig, E. Giannini, A. F. Morpurgo, *Nat. Commun.* **2015**, *6*, 8892.
[23] L. Thoutam, Y. Wang, Z. Xiao, S. Das, A. Luican-Mayer, R. Divan, G. Crabtree, W. Kwok, *Phys. Rev. Lett.* **2015**, *115*, 046602.
[24] X. Qian, J. Liu, L. Fu, J. Li, *Science* **2014**, *346*, 1344.
[25] Z. Fei, T. Palomaki, S. Wu, W. Zhao, X. Cai, B. Sun, P. Nguyen, J. Finney, X. Xu, D. H. Cobden, *Nat. Phys.* **2017**, *13*, 677.
[26] D. H. Keum, S. Cho, J. H. Kim, D.-H. Choe, H.-J. Sung, M. Kan, H. Kang, J.-Y. Hwang, S. W. Kim, H. Yang, *Nat. Phys.* **2015**, *11*, 482.
[27] X. Yu, P. Yu, D. Wu, B. Singh, Q. Zeng, H. Lin, W. Zhou, J. Lin, K. Suenaga, Z. Liu, *Nat. Commun.* **2018**, *9*, 1545.
[28] Y. Zhao, J. Qiao, P. Yu, Z. Hu, Z. Lin, S. P. Lau, Z. Liu, W. Ji, Y. Chai, *Adv. Mater.* **2016**, *28*, 2399.
[29] L. Li, W. Wang, Y. Chai, H. Li, M. Tian, T. Zhai, *Adv. Funct. Mater.* **2017**, *27*, 1701011.
[30] Y. Wang, L. Li, W. Yao, S. Song, J. Sun, J. Pan, X. Ren, C. Li, E. Okunishi, Y.-Q. Wang, E. Wang, Y. Shao, Y. Y. Zhang, H.-T. Yang, E. F. Schwier, H. Iwasawa, K. Shimada, M. Taniguchi, Z. Cheng, S. Zhou, S. Du, S. J. Pennycook, S. T. Pantelides, H.-J. Gao, *Nano Lett.* **2015**, *15*, 4013.
[31] Y. Zhao, J. Qiao, Z. Yu, P. Yu, K. Xu, S. P. Lau, W. Zhou, Z. Liu, X. Wang, W. Ji, *Adv. Mater.* **2017**, *29*, 1604230.
[32] W. Jie, X. Chen, D. Li, L. Xie, Y. Y. Hui, S. P. Lau, X. Cui, J. Hao, *Angew. Chem. Int. Ed.* **2015**, *54*, 1185.
[33] R. Longuinhos, J. Ribeiro-Soares, *Phys. Chem. Chem. Phys.* **2016**, *18*, 25401.
[34] J. J. Fonseca, S. Tongay, M. Topsakal, A. R. Chew, A. J. Lin, C. Ko, A. V. Luce, A. Salleo, J. Wu, O. D. Dubon, *Adv. Mater.* **2016**, *28*, 6465.
[35] H. Li, X. Han, D. Pan, X. Yan, H.-W. Wang, C. Wu, G. Cheng, H. Zhang, S. Yang, B. Li, H. He, J. Wang, *Cryst. Growth Des.* **2018**, *18*, 2899.
[36] X. Li, L. Basile, M. Yoon, C. Ma, A. A. Puretzky, J. Lee, J. C. Idrobo, M. Chi, C. M. Rouleau, D. B. Geohegan, K. Xiao, *Angew. Chem. Int. Ed.* **2015**, *54*, 2712.
[37] M. J. Hamer, E. Tóvári, M. Zhu, M. D. Thompson, A. S. Mayorov, J. Prance, Y. Lee, R. P. Haley, Z. R. Kudrynskyi, A. Patanè, D. Terry, Z. D. Kovalyuk, K. Ensslin, A. V. Kretinin, A. Geim, R. Gorbachev, *Nano Lett.* **2018**, *18*, 3950.
[38] P. Hu, Z. Wen, L. Wang, P. Tan, K. Xiao, *ACS Nano* **2012**, *6*, 5988.
[39] G. W. Mudd, M. R. Molas, X. Chen, V. Zólyomi, K. Nogajewski, Z. R. Kudrynskyi, Z. D. Kovalyuk, G. Yusa, O. Makarovsky, L. Eaves, M. Potemski, V. I. Fal'ko, A. Patanè, *Sci. Rep.* **2016**, *6*, 39619.
[40] G. W. Mudd, S. A. Svatek, T. Ren, A. Patanè, O. Makarovsky, L. Eaves, P. H. Beton, Z. D. Kovalyuk, G. V. Lashkarev, Z. R. Kudrynskyi, *Adv. Mater.* **2013**, *25*, 5714.
[41] Y. Yi, X.-F. Yu, W. Zhou, J. Wang, P. K. Chu, *Mater. Sci. Eng. R: Rep.* **2017**, *120*, 1.
[42] V. Tran, R. Soklaski, Y. Liang, L. Yang, *Phys. Rev. B* **2014**, *89*, 235319.
[43] T. Low, A. Rodin, A. Carvalho, Y. Jiang, H. Wang, F. Xia, A. C. Neto, *Phys. Rev. B* **2014**, *90*, 075434.
[44] J. Qiao, X. Kong, Z.-X. Hu, F. Yang, W. Ji, *Nat. Commun.* **2014**, *5*, 4475.
[45] D. Xiao, G.-B. Liu, W. Feng, X. Xu, W. Yao, *Phys. Rev. Lett.* **2012**, *108*, 196802.
[46] X. Xu, W. Yao, D. Xiao, T. F. Heinz, *Nat. Phys.* **2014**, *10*, 343.
[47] K. F. Mak, D. Xiao, J. Shan, *Nat. Photonics* **2018**, *12*, 451.
[48] F. H. L. Koppens, T. Mueller, P. Avouris, A. C. Ferrari, M. S. Vitiello, M. Polini, *Nat. Nanotechnol.* **2014**, *9*, 780.
[49] D. Xiao, W. Yao, Q. Niu, *Phys. Rev. Lett.* **2007**, *99*, 236809.
[50] W. Yao, D. Xiao, Q. Niu, *Phys. Rev. B* **2008**, *77*, 235406.
[51] W. Feng, Y. Yao, W. Zhu, J. Zhou, W. Yao, D. Xiao, *Phys. Rev. B* **2012**, *86*, 165108.
[52] R. Gorbachev, J. Song, G. Yu, A. Kretinin, F. Withers, Y. Cao, A. Mishchenko, I. Grigorieva, K. Novoselov, L. Levitov, A. K. Geim, *Science* **2014**, *346*, 448.
[53] K. F. Mak, K. L. McGill, J. Park, P. L. McEuen, *Science* **2014**, *344*, 1489.
[54] J. Lee, K. F. Mak, J. Shan, *Nat. Nanotechnol.* **2016**, *11*, 421.
[55] M. Sui, G. Chen, L. Ma, W.-Y. Shan, D. Tian, K. Watanabe, T. Taniguchi, X. Jin, W. Yao, D. Xiao, Y. Zhang, *Nat. Phys.* **2015**, *11*, 1027.
[56] Y. Shimazaki, M. Yamamoto, I. V. Borzenets, K. Watanabe, T. Taniguchi, S. Tarucha, *Nat. Phys.* **2015**, *11*, 1032.
[57] J. Li, K. Wang, K. J. McFaul, Z. Zern, Y. Ren, K. Watanabe, T. Taniguchi, Z. Qiao, J. Zhu, *Nat. Nanotechnol.* **2016**, *11*, 1060.

[58] K. F. Mak, J. Shan, *Nat. Photonics* **2016**, *10*, 216.
[59] M. Onga, Y. Zhang, T. Ideue, Y. Iwasa, *Nat. Mater.* **2017**, *16*, 1193.
[60] Z. Ye, D. Sun, T. F. Heinz, *Nat. Phys.* **2016**, *13*, 26.
[61] H. Yu, X. Cui, X. Xu, W. Yao, *Natl. Sci. Rev.* **2015**, *2*, 57.
[62] K. He, N. Kumar, L. Zhao, Z. Wang, K. F. Mak, H. Zhao, J. Shan, *Phys. Rev. Lett.* **2014**, *113*, 026803.
[63] A. Chernikov, T. C. Berkelbach, H. M. Hill, A. Rigosi, Y. Li, O. B. Aslan, D. R. Reichman, M. S. Hybertsen, T. F. Heinz, *Phys. Rev. Lett.* **2014**, *113*, 076802.
[64] D. Y. Qiu, F. H. da Jornada, S. G. Louie, *Phys. Rev. Lett.* **2013**, *111*, 216805.
[65] H. Zeng, J. Dai, W. Yao, D. Xiao, X. Cui, *Nat. Nanotechnol.* **2012**, *7*, 490.
[66] K. F. Mak, K. He, J. Shan, T. F. Heinz, *Nat. Nanotechnol.* **2012**, *7*, 494.
[67] T. Cao, G. Wang, W. Han, H. Ye, C. Zhu, J. Shi, Q. Niu, P. Tan, E. Wang, B. Liu, J. Feng, *Nat. Commun.* **2012**, *3*, 887.
[68] A. M. Jones, H. Yu, N. J. Ghimire, S. Wu, G. Aivazian, J. S. Ross, B. Zhao, J. Yan, D. G. Mandrus, D. Xiao, W. Yao, X. Xu, *Nat. Nanotechnol.* **2013**, *8*, 634.
[69] G. Sallen, L. Bouet, X. Marie, G. Wang, C. Zhu, W. Han, Y. Lu, P. Tan, T. Amand, B. Liu, *Phys. Rev. B* **2012**, *86*, 081301.
[70] Y. Zhang, T. Oka, R. Suzuki, J. Ye, Y. Iwasa, *Science* **2014**, *344*, 725.
[71] J. S. Ross, P. Klement, A. M. Jones, N. J. Ghimire, J. Yan, D. G. Mandrus, T. Taniguchi, K. Watanabe, K. Kitamura, W. Yao, D. H. Cobden, X. Xu, *Nat. Nanotechnol.* **2014**, *9*, 268.
[72] M. Onga, Y. Zhang, R. Suzuki, Y. Iwasa, *Appl. Phys. Lett.* **2016**, *108*, 073107.
[73] G. Aivazian, Z. Gong, A. M. Jones, R.-L. Chu, J. Yan, D. G. Mandrus, C. Zhang, D. Cobden, W. Yao, X. Xu, *Nat. Phys.* **2015**, *11*, 148.
[74] A. Srivastava, M. Sidler, A. V. Allain, D. S. Lembke, A. Kis, A. Imamoğlu, *Nat. Phys.* **2015**, *11*, 141.
[75] Y. Li, J. Ludwig, T. Low, A. Chernikov, X. Cui, G. Arefe, Y. D. Kim, A. M. van der Zande, A. Rigosi, H. M. Hill, S. H. Kim, J. Hone, Z. Li, D. Smirnov, T. F. Heinz, *Phys. Rev. Lett.* **2014**, *113*, 266804.
[76] A. V. Stier, K. M. McCreary, B. T. Jonker, J. Kono, S. A. Crooker, *Nat. Commun.* **2016**, *7*, 10643.
[77] K. L. Seyler, D. Zhong, B. Huang, X. Linpeng, N. P. Wilson, T. Taniguchi, K. Watanabe, W. Yao, D. Xiao, M. A. McGuire, K.-M. C. Fu, X. Xu, *Nano Lett.* **2018**, *18*, 3823.
[78] C. Zhao, T. Norden, P. Zhang, P. Zhao, Y. Cheng, F. Sun, J. P. Parry, P. Taheri, J. Wang, Y. Yang, T. Scrace, K. Kang, S. Yang, G. X. Miao, R. Sabirianov, G. Kioseoglou, W. Huang, A. Petrou, H. Zeng, *Nat. Nanotechnol.* **2017**, *12*, 757.
[79] J. Lee, Z. Wang, H. Xie, K. F. Mak, J. Shan, *Nat. Mater.* **2017**, *16*, 887.
[80] H. Yu, W. Yao, *Nat. Mater.* **2017**, *16*, 876.
[81] A. M. Jones, H. Yu, J. S. Ross, P. Klement, N. J. Ghimire, J. Yan, D. G. Mandrus, W. Yao, X. Xu, *Nat. Phys.* **2014**, *10*, 130.
[82] H. Yuan, M. S. Bahramy, K. Morimoto, S. Wu, K. Nomura, B.-J. Yang, H. Shimotani, R. Suzuki, M. Toh, C. Kloc, X. Xu, R. Arita, N. Nagaosa, Y. Iwasa, *Nat. Phys.* **2013**, *9*, 563.
[83] X. Chen, T. Yan, B. Zhu, S. Yang, X. Cui, *ACS Nano* **2017**, *11*, 1581.
[84] Z. Gong, G.-B. Liu, H. Yu, D. Xiao, X. Cui, X. Xu, W. Yao, *Nat. Commun.* **2013**, *4*, 2053.
[85] B. Zhu, H. Zeng, J. Dai, Z. Gong, X. Cui, *Proc. Natl. Acad. Sci. USA* **2014**, *111*, 11606.
[86] P. Rivera, J. R. Schaibley, A. M. Jones, J. S. Ross, S. Wu, G. Aivazian, P. Klement, K. Seyler, G. Clark, N. J. Ghimire, J. Yan, D. G. Mandrus, W. Yao, X. Xu, *Nat. Commun.* **2015**, *6*, 6242.
[87] P. Rivera, K. L. Seyler, H. Yu, J. R. Schaibley, J. Yan, D. G. Mandrus, W. Yao, X. Xu, *Science* **2016**, *351*, 688.
[88] C. Mai, A. Barrette, Y. Yu, Y. G. Semenov, K. W. Kim, L. Cao, K. Gundogdu, *Nano Lett.* **2014**, *14*, 202.
[89] G. Wang, L. Bouet, D. Lagarde, M. Vidal, A. Balocchi, T. Amand, X. Marie, B. Urbaszek, *Phys. Rev. B* **2014**, *90*, 075413.
[90] W.-T. Hsu, Y.-L. Chen, C.-H. Chen, P.-S. Liu, T.-H. Hou, L.-J. Li, W.-H. Chang, *Nat. Commun.* **2015**, *6*, 8963.
[91] T. Yan, J. Ye, X. Qiao, P. Tan, X. Zhang, *Phys. Chem. Chem. Phys.* **2017**, *19*, 3176.
[92] L. Yang, N. A. Sinitsyn, W. Chen, J. Yuan, J. Zhang, J. Lou, S. A. Crooker, *Nat. Phys.* **2015**, *11*, 830.
[93] S. Dal Conte, F. Bottegoni, E. A. A. Pogna, D. De Fazio, S. Ambrogio, I. Bargigia, C. D'Andrea, A. Lombardo, M. Bruna, F. Ciccacci, A. C. Ferrari, G. Cerullo, M. Finazzi, *Phys. Rev. B* **2015**, *92*, 235425.
[94] D. Lagarde, L. Bouet, X. Marie, C. Zhu, B. Liu, T. Amand, P. Tan, B. Urbaszek, *Phys. Rev. Lett.* **2014**, *112*, 047401.
[95] T. Yu, M. Wu, *Phys. Rev. B* **2014**, *89*, 205303.
[96] M. Glazov, T. Amand, X. Marie, D. Lagarde, L. Bouet, B. Urbaszek, *Phys. Rev. B* **2014**, *89*, 201302.
[97] K. Novoselov, A. Mishchenko, A. Carvalho, A. C. Neto, *Science* **2016**, *353*, aac9439.
[98] Y. Liu, N. O. Weiss, X. Duan, H.-C. Cheng, Y. Huang, X. Duan, *Nat. Rev. Mater.* **2016**, *1*, 16042.
[99] J. Kunstmann, F. Mooshammer, P. Nagler, A. Chaves, F. Stein, N. Paradiso, G. Plechinger, C. Strunk, C. Schüller, G. Seifert, D. R. Reichman, T. Korn, *Nat. Phys.* **2018**, *14*, 801.
[100] A. Surrente, Ł. Kłopotowski, N. Zhang, M. Baranowski, A. A. Mitioglu, M. V. Ballottin, P. C. M. Christianen, D. Dumcenco, Y.-C. Kung, D. K. Maude, A. Kis, P. Plochocka, *Nano Lett.* **2018**, *18*, 3994.
[101] M. Palummo, M. Bernardi, J. C. Grossman, *Nano Lett.* **2015**, *15*, 2794.
[102] P. Rivera, H. Yu, K. L. Seyler, N. P. Wilson, W. Yao, X. Xu, *Nat. Nanotechnol.* **2018**, *13*, 1004.
[103] A. K. Geim, I. V. Grigorieva, *Nature* **2013**, *499*, 419.
[104] R. Cheng, D. Li, H. Zhou, C. Wang, A. Yin, S. Jiang, Y. Liu, Y. Chen, Y. Huang, X. Duan, *Nano Lett.* **2014**, *14*, 5590.
[105] H. Fang, C. Battaglia, C. Carraro, S. Nemsak, B. Ozdol, J. S. Kang, H. A. Bechtel, S. B. Desai, F. Kronast, A. A. Unal, *Proc. Natl. Acad. Sci. USA* **2014**, *111*, 6198.
[106] M.-H. Chiu, M.-Y. Li, W. Zhang, W.-T. Hsu, W.-H. Chang, M. Terrones, H. Terrones, L.-J. Li, *ACS Nano* **2014**, *8*, 9649.
[107] X. Hong, J. Kim, S.-F. Shi, Y. Zhang, C. Jin, Y. Sun, S. Tongay, J. Wu, Y. Zhang, F. Wang, *Nat. Nanotechnol.* **2014**, *9*, 682.
[108] F. Ceballos, M. Z. Bellus, H.-Y. Chiu, H. Zhao, *ACS Nano* **2014**, *8*, 12717.
[109] T. Deilmann, K. S. Thygesen, *Nano Lett.* **2018**, *18*, 1460.
[110] J. R. Schaibley, P. Rivera, H. Yu, K. L. Seyler, J. Yan, D. G. Mandrus, T. Taniguchi, K. Watanabe, W. Yao, X. Xu, *Nat. Commun.* **2016**, *7*, 13747.
[111] C.-H. Lee, G.-H. Lee, A. M. Van Der Zande, W. Chen, Y. Li, M. Han, X. Cui, G. Arefe, C. Nuckolls, T. F. Heinz, *Nat. Nanotechnol.* **2014**, *9*, 676.
[112] S. D. Sarma, A. Pinczuk, *Perspectives in quantum Hall effects: Novel quantum liquids in low-dimensional semiconductor structures*, Wiley-VCH, Weinheim **2008**.
[113] S. M. Girvin, in *Aspects topologiques de la physique en basse dimension. Topological Aspects of Low Dimensional Systems* (Eds: A. Comtet, T. Jolicoeur, S. Ouvry, F. David), Springer, Berlin **1999**.
[114] Y. Zhang, Y.-W. Tan, H. L. Stormer, P. Kim, *Nature* **2005**, *438*, 201.
[115] A. Stern, *Ann. Phys.* **2008**, *323*, 204.
[116] K. S. Novoselov, A. K. Geim, S. V. Morozov, D. Jiang, M. I. Katsnelson, I. V. Grigorieva, S. V. Dubonos, A. A. Firsov, *Nature* **2005**, *438*, 197.
[117] V. Gusynin, S. Sharapov, *Phys. Rev. Lett.* **2005**, *95*, 146801.
[118] J. G. Checkelsky, L. Li, N. P. Ong, *Phys. Rev. Lett.* **2008**, *100*, 206801.
[119] Y. Zhang, Z. Jiang, J. P. Small, M. S. Purewal, Y. W. Tan, M. Fazlollahi, J. D. Chudow, J. A. Jaszczak, H. L. Stormer, P. Kim, *Phys. Rev. Lett.* **2006**, *96*, 136806.

[120] K. I. Bolotin, F. Ghahari, M. D. Shulman, H. L. Stormer, P. Kim, *Nature* **2009**, *462*, 196.
[121] J. I. A. Li, C. Tan, S. Chen, Y. Zeng, T. Taniguchi, K. Watanabe, J. Hone, C. R. Dean, *Science* **2017**, *358*, 648.
[122] G. Diankov, C.-T. Liang, F. Amet, P. Gallagher, M. Lee, A. J. Bestwick, K. Tharratt, W. Coniglio, J. Jaroszynski, K. Watanabe, *Nat. Commun.* **2016**, *7*, 13908.
[123] P. Maher, L. Wang, Y. Gao, C. Forsythe, T. Taniguchi, K. Watanabe, D. Abanin, Z. Papić, P. Cadden-Zimansky, J. Hone, P. Kim, C. R. Dean, *Science* **2014**, *345*, 61.
[124] J. D. Sanchez-Yamagishi, J. Y. Luo, A. F. Young, B. M. Hunt, K. Watanabe, T. Taniguchi, R. C. Ashoori, P. Jarillo-Herrero, *Nat. Nanotechnol.* **2017**, *12*, 118.
[125] A. F. Young, J. D. Sanchez-Yamagishi, B. Hunt, S. H. Choi, K. Watanabe, T. Taniguchi, R. C. Ashoori, P. Jarillo-Herrero, *Nature* **2014**, *505*, 528.
[126] M. Zhang, X. Wang, F. Song, R. Zhang, *Adv. Quantum Technol.* **2019**, *2*, 1800039.
[127] B. A. Bernevig, S.-C. Zhang, *Phys. Rev. Lett.* **2006**, *96*, 106802.
[128] C. L. Kane, E. J. Mele, *Phys. Rev. Lett.* **2005**, *95*, 226801.
[129] C. L. Kane, E. J. Mele, *Phys. Rev. Lett.* **2005**, *95*, 146802.
[130] A. F. Young, C. R. Dean, L. Wang, H. Ren, P. Cadden-Zimansky, K. Watanabe, T. Taniguchi, J. Hone, K. L. Shepard, P. Kim, *Nat. Phys.* **2012**, *8*, 550.
[131] D. A. Abanin, P. A. Lee, L. S. Levitov, *Phys. Rev. Lett.* **2006**, *96*, 176803.
[132] P. Maher, C. R. Dean, A. F. Young, T. Taniguchi, K. Watanabe, K. L. Shepard, J. Hone, P. Kim, *Nat. Phys.* **2013**, *9*, 154.
[133] J. Velasco Jr, L. Jing, W. Bao, Y. Lee, P. Kratz, V. Aji, M. Bockrath, C. N. Lau, C. Varma, R. Stillwell, D. Smirnov, F. Zhang, J. Jung, A. H. MacDonald, *Nat. Nanotechnol.* **2012**, *7*, 156.
[134] E. V. Gorbar, V. P. Gusynin, V. A. Miransky, *Phys. Rev. B* **2010**, *81*, 155451.
[135] F. Freitag, J. Trbovic, M. Weiss, C. Schönenberger, *Phys. Rev. Lett.* **2012**, *108*, 076602.
[136] M. Kharitonov, *Phys. Rev. Lett.* **2012**, *109*, 046803.
[137] F. Finocchiaro, F. Guinea, P. San-Jose, *2D Mater.* **2017**, *4*, 025027.
[138] P. Stepanov, S. Che, D. Shcherbakov, J. Yang, R. Chen, K. Thilahar, G. Voigt, M. W. Bockrath, D. Smirnov, K. Watanabe, T. Taniguchi, R. K. Lake, Y. Barlas, A. H. MacDonald, C. N. Lau, *Nat. Phys.* **2018**, *14*, 907.
[139] X. Cui, G.-H. Lee, Y. D. Kim, G. Arefe, P. Y. Huang, C.-H. Lee, D. A. Chenet, X. Zhang, L. Wang, F. Ye, F. Pizzocchero, B. S. Jessen, K. Watanabe, T. Taniguchi, D. A. Muller, T. Low, P. Kim, J. Hone, *Nat. Nanotechnol.* **2015**, *10*, 534.
[140] L. Li, F. Yang, G. J. Ye, Z. Zhang, Z. Zhu, W. Lou, X. Zhou, L. Li, K. Watanabe, T. Taniguchi, K. Chang, Y. Wang, X. H. Chen, Y. Zhang, *Nat. Nanotechnol.* **2016**, *11*, 593.
[141] Z. Wu, S. Xu, H. Lu, A. Khamoshi, G.-B. Liu, T. Han, Y. Wu, J. Lin, G. Long, Y. He, Y. Cai, Y. Yao, F. Zhang, N. Wang, *Nat. Commun.* **2016**, *7*, 12955.
[142] H. C. P. Movva, B. Fallahazad, K. Kim, S. Larentis, T. Taniguchi, K. Watanabe, S. K. Banerjee, E. Tutuc, *Phys. Rev. Lett.* **2017**, *118*, 247701.
[143] D. Jariwala, V. K. Sangwan, L. J. Lauhon, T. J. Marks, M. C. Hersam, *ACS Nano* **2014**, *8*, 1102.
[144] W. Feng, W. Zheng, W. Cao, P. Hu, *Adv. Mater.* **2014**, *26*, 6587.
[145] S. Sucharitakul, N. J. Goble, U. R. Kumar, R. Sankar, Z. A. Bogorad, F.-C. Chou, Y.-T. Chen, X. P. A. Gao, *Nano Lett.* **2015**, *15*, 3815.
[146] S. Datta, *Electronic Transport in Mesoscopic Systems*, Cambridge University Press, Cambridge **1997**.
[147] N. Ma, D. Jena, *Phys. Rev. X* **2014**, *4*, 011043.
[148] B. Radisavljevic, A. Kis, *Nat. Mater.* **2013**, *12*, 815.
[149] H. Fang, S. Chuang, T. C. Chang, K. Takei, T. Takahashi, A. Javey, *Nano Lett.* **2012**, *12*, 3788.
[150] D. Xiang, C. Han, J. Wu, S. Zhong, Y. Liu, J. Lin, X.-A. Zhang, W. Ping Hu, B. Özyilmaz, A. H. C. Neto, A. T. S. Wee, W. Chen, *Nat. Commun.* **2015**, *6*, 6485.
[151] Z. Ye, L. Waldecker, E. Y. Ma, D. Rhodes, A. Antony, B. Kim, X. X. Zhang, M. Deng, Y. Jing, Z. Lu, D. Smirnov, K. Watanabe, T. Taniguchi, J. Hone, T. F. Heinz, *Nat. Commun.* **2018**, *9*, 3718.
[152] S. Xu, Z. Wu, H. Lu, Y. Han, G. Long, X. Chen, T. Han, W. Ye, Y. Wu, J. Lin, *2D Mater.* **2016**, *3*, 021007.
[153] G. Long, D. Maryenko, J. Shen, S. Xu, J. Hou, Z. Wu, W. K. Wong, T. Han, J. Lin, Y. Cai, *Nano Lett.* **2016**, *16*, 7768.
[154] D. Shoenberg, *Magnetic Oscillations in Metals*, Cambridge University Press, Cambridge **2009**.
[155] G. Long, D. Maryenko, S. Pezzini, S. Xu, Z. Wu, T. Han, J. Lin, C. Cheng, Y. Cai, U. Zeitler, N. Wang, *Phys. Rev. B* **2017**, *96*, 155448.
[156] L. Li, G. J. Ye, V. Tran, R. Fei, G. Chen, H. Wang, J. Wang, K. Watanabe, T. Taniguchi, L. Yang, X. H. Chen, Y. Zhang, *Nat. Nanotechnol.* **2015**, *10*, 608.
[157] X. Chen, Y. Wu, Z. Wu, Y. Han, S. Xu, L. Wang, W. Ye, T. Han, Y. He, Y. Cai, *Nat. Commun.* **2015**, *6*, 7315.
[158] B. Fallahazad, H. C. P. Movva, K. Kim, S. Larentis, T. Taniguchi, K. Watanabe, S. K. Banerjee, E. Tutuc, *Phys. Rev. Lett.* **2016**, *116*, 086601.
[159] M. Yankowitz, D. McKenzie, B. J. LeRoy, *Phys. Rev. Lett.* **2015**, *115*, 136803.
[160] Y. Zhang, M. M. Ugeda, C. Jin, S.-F. Shi, A. J. Bradley, A. Martín-Recio, H. Ryu, J. Kim, S. Tang, Y. Kim, B. Zhou, C. Hwang, Y. Chen, F. Wang, M. F. Crommie, Z. Hussain, Z.-X. Shen, S.-K. Mo, *Nano Lett.* **2016**, *16*, 2485.
[161] S. Xu, J. Shen, G. Long, Z. Wu, Z.-q. Bao, C.-C. Liu, X. Xiao, T. Han, J. Lin, Y. Wu, H. Lu, J. Hou, L. An, Y. Wang, Y. Cai, K. M. Ho, Y. He, R. Lortz, F. Zhang, N. Wang, *Phys. Rev. Lett.* **2017**, *118*, 067702.
[162] Q. H. Chen, J. M. Lu, L. Liang, O. Zheliuk, A. Ali, P. Sheng, J. T. Ye, *Phys. Rev. Lett.* **2017**, *119*, 147002.
[163] R. Pisoni, Y. Lee, H. Overweg, M. Eich, P. Simonet, K. Watanabe, T. Taniguchi, R. Gorbachev, T. Ihn, K. Ensslin, *Nano Lett.* **2017**, *17*, 5008.
[164] S. Tang, C. Zhang, D. Wong, Z. Pedramrazi, H.-Z. Tsai, C. Jia, B. Moritz, M. Claassen, H. Ryu, S. Kahn, J. Jiang, H. Yan, M. Hashimoto, D. Lu, R. G. Moore, C.-C. Hwang, C. Hwang, Z. Hussain, Y. Chen, M. M. Ugeda, Z. Liu, X. Xie, T. P. Devereaux, M. F. Crommie, S.-K. Mo, Z.-X. Shen, *Nat. Phys.* **2017**, *13*, 683.
[165] F. Xia, H. Wang, D. Xiao, M. Dubey, A. Ramasubramaniam, *Nat. Photonics* **2014**, *8*, 899.
[166] Z. Sun, A. Martinez, F. Wang, *Nat. Photonics* **2016**, *10*, 227.
[167] G. Fiori, F. Bonaccorso, G. Iannaccone, T. Palacios, D. Neumaier, A. Seabaugh, S. K. Banerjee, L. Colombo, *Nat. Nanotechnol.* **2014**, *9*, 768.
[168] S. Wu, V. Fatemi, Q. D. Gibson, K. Watanabe, T. Tagiguchi, R. J. Cava, P. Jarillo-Herrero, *Science* **2018**, *359*, 76.
[169] Z. Song, Z. Li, H. Wang, X. Bai, W. Wang, H. Du, S. Liu, C. Wang, J. Han, Y. Yang, Z. Liu, J. Lu, Z. Fang, J. Yang, *Nano Lett.* **2017**, *17*, 2079.
[170] R. V. Gorbachev, A. K. Geim, M. I. Katsnelson, K. S. Novoselov, T. Tudorovskiy, I. V. Grigorieva, A. H. MacDonald, S. V. Morozov, K. Watanabe, T. Taniguchi, L. A. Ponomarenko, *Nat. Phys.* **2012**, *8*, 896.
[171] Z. Song, C. C. Liu, J. Yang, J. Han, M. Ye, B. Fu, Y. Yang, Q. Niu, J. Lu, Y. Yao, *NPG Asia Mater.* **2014**, *6*, e147.
[172] R. L. Chu, X. Li, S. Wu, Q. Niu, W. Yao, X. Xu, C. Zhang, *Phys. Rev. B* **2014**, *90*, 045427.
[173] B. Huang, G. Clark, D. R. Klein, D. MacNeill, E. Navarro-Moratalla, K. L. Seyler, N. Wilson, M. A. McGuire, D. H. Cobden, D. Xiao, W. Yao, P. Jarillo-Herrero, X. Xu, *Nat. Nanotechnol.* **2018**, *13*, 544.
[174] K. S. Burch, D. Mandrus, J. G. Park, *Nature* **2018**, *563*, 47.

[175] N. Sivadas, S. Okamoto, X. Xu, C. J. Fennie, D. Xiao, *Nano Lett.* **2018**, *18*, 7658.
[176] B. Huang, G. Clark, E. Navarro-Moratalla, D. R. Klein, R. Cheng, K. L. Seyler, D. Zhong, E. Schmidgall, M. A. McGuire, D. H. Cobden, W. Yao, D. Xiao, P. Jarillo-Herrero, X. Xu, *Nature* **2017**, *546*, 270.
[177] T. Song, X. Cai, M. W.-Y. Tu, X. Zhang, B. Huang, N. P. Wilson, K. L. Seyler, L. Zhu, T. Taniguchi, K. Watanabe, M. A. McGuire, D. H. Cobden, D. Xiao, W. Yao, X. Xu, *Science* **2018**, *360*, 1214.
[178] D. Zhong, K. L. Seyler, X. Linpeng, R. Cheng, N. Sivadas, B. Huang, E. Schmidgall, T. Taniguchi, K. Watanabe, M. A. McGuire, W. Yao, D. Xiao, K.-M. C. Fu, X. Xu, *Sci. Adv.* **2017**, *3*, e1603113.
[179] X. Li, T. Cao, Q. Niu, J. Shi, J. Feng, *Proc. Natl. Acad. Sci. USA* **2013**, *110*, 3738.
[180] W. Y. Tong, S. J. Gong, X. Wan, C. G. Duan, *Nat. Commun.* **2016**, *7*, 13612.
[181] Z. Song, X. Sun, J. Zheng, F. Pan, Y. Hou, M. H. Yung, J. Yang, J. Lu, *Nanoscale* **2018**, *10*, 13986.
[182] Y. Lai, Z. Song, Y. Wan, M. Xue, C. Wang, Y. Ye, L. Dai, Z. Zhang, W. Yang, H. Du, J. Yang, *Nanoscale* **2019**, *11*, 5163.
[183] M. Massicotte, P. Schmidt, F. Vialla, K. G. Schädler, A. Reserbat-Plantey, K. Watanabe, T. Taniguchi, K.-J. Tielrooij, F. H. Koppens, *Nat. Nanotechnol.* **2016**, *11*, 42.
[184] L. Britnell, R. Ribeiro, A. Eckmann, R. Jalil, B. Belle, A. Mishchenko, Y.-J. Kim, R. Gorbachev, T. Georgiou, S. Morozov, *Science* **2013**, *340*, 1311.
[185] W. J. Yu, Y. Liu, H. Zhou, A. Yin, Z. Li, Y. Huang, X. Duan, *Nat. Nanotechnol.* **2013**, *8*, 952.
[186] Y. Deng, Z. Luo, N. J. Conrad, H. Liu, Y. Gong, S. Najmaei, P. M. Ajayan, J. Lou, X. Xu, P. D. Ye, *ACS Nano* **2014**, *8*, 8292.
[187] F. Wang, Z. Wang, K. Xu, F. Wang, Q. Wang, Y. Huang, L. Yin, J. He, *Nano Lett.* **2015**, *15*, 7558.
[188] M. M. Furchi, A. Pospischil, F. Libisch, J. Burgdörfer, T. Mueller, *Nano Lett.* **2014**, *14*, 4785.
[189] F. Withers, O. Del Pozo-Zamudio, A. Mishchenko, A. P. Rooney, A. Gholinia, K. Watanabe, T. Taniguchi, S. J. Haigh, A. K. Geim, A. I. Tartakovskii, K. S. Novoselov, *Nat. Mater.* **2015**, *14*, 301.
[190] F. Withers, O. Del Pozo-Zamudio, S. Schwarz, S. Dufferwiel, P. M. Walker, T. Godde, A. P. Rooney, A. Gholinia, C. R. Woods, P. Blake, S. J. Haigh, K. Watanabe, T. Taniguchi, I. L. Aleiner, A. K. Geim, V. I. Fal'ko, A. I. Tartakovskii, K. S. Novoselov, *Nano Lett.* **2015**, *15*, 8223.
[191] Y. Ye, J. Xiao, H. Wang, Z. Ye, H. Zhu, M. Zhao, Y. Wang, J. Zhao, X. Yin, X. Zhang, *Nat. Nanotechnol.* **2016**, *11*, 598.
[192] M. Eginligil, B. Cao, Z. Wang, X. Shen, C. Cong, J. Shang, C. Soci, T. Yu, *Nat. Commun.* **2015**, *6*, 7636.
[193] L. Xie, X. Cui, *Proc. Natl. Acad. Sci. USA* **2016**, *113*, 3746.
[194] H. J. Kimble, *Nature* **2008**, *453*, 1023.
[195] G. Khitrova, H. M. Gibbs, M. Kira, S. W. Koch, A. Scherer, *Nat. Phys.* **2006**, *2*, 81.
[196] D. Xu, X. Xiong, L. Wu, X.-F. Ren, C. E. Png, G.-C. Guo, Q. Gong, Y.-F. Xiao, *Adv. Opt. Photonics* **2018**, *10*, 703.
[197] B. Kolaric, B. Maes, K. Clays, T. Durt, Y. Caudano, *Adv. Quantum Technol.* **2018**, *1*, 1800001.
[198] R. Liu, Z. K. Zhou, Y. C. Yu, T. Zhang, H. Wang, G. Liu, Y. Wei, H. Chen, X. H. Wang, *Phys. Rev. Lett.* **2017**, *118*, 237401.
[199] P. Peng, Y. C. Liu, D. Xu, Q. T. Cao, G. Lu, Q. Gong, X. F. Xiao, *Phys. Rev. Lett.* **2017**, *119*, 233901.
[200] T. Song, Z. Chen, W. Zhang, L. Lin, Y. Bao, L. Wu, Z. K. Zhou, *Nanomaterials* **2019**, *9*, 564.
[201] D. G. Baranov, M. Wersäll, J. Cuadra, T. J. Antosiewicz, T. Shegai, *ACS Photonics* **2018**, *5*, 24.
[202] E. J. Sie, J. W. McIver, Y.-H. Lee, L. Fu, J. Kong, N. Gedik, *Nat. Mater.* **2015**, *14*, 290.
[203] J. Wen, H. Wang, W. Wang, Z. Deng, C. Zhuang, Y. Zhang, F. Liu, J. She, J. Chen, H. Chen, S. Deng, N. Xu, *Nano Lett.* **2017**, *17*, 4689.
[204] J. Cuadra, D. G. Baranov, M. Wersäll, R. Verre, T. J. Antosiewicz, T. Shegai, *Nano Lett.* **2018**, *18*, 1777.
[205] M.-E. Kleemann, R. Chikkaraddy, E. M. Alexeev, D. Kos, C. Carnegie, W. Deacon, A. C. de Pury, C. Große, B. de Nijs, J. Mertens, A. I. Tartakovskii, J. J. Baumberg, *Nat. Commun.* **2017**, *8*, 1296.
[206] M. Stührenberg, B. Munkhbat, D. G. Baranov, J. Cuadra, A. B. Yankovich, T. J. Antosiewicz, E. Olsson, T. Shegai, *Nano Lett.* **2018**, *18*, 5938.
[207] X. Liu, T. Galfsky, Z. Sun, F. Xia, E. C. Lin, Y. H. Lee, S. Kéna-Cohen, V. M. Menon, *Nat. Photonics* **2015**, *9*, 30.
[208] S. Dufferwiel, S. Schwarz, F. Withers, A. A. P. Trichet, F. L. M. Sich, O. Del Pozo-Zamudio, C. Clark, A. Nalitov, D. D. Solnyshkov, G. Malpuech, K. S. Novoselov, J. M. Smith, M. S. Skolnick, D. N. Krizhanovskii, A. I. Tartakovskii, *Nat. Commun.* **2015**, *6*, 8579.
[209] S. Wang, S. Li, T. Chervy, A. Shalabney, S. Azzini, E. Orgiu, J. A. Hutchison, C. Genet, P. Samorì, T. W. Ebbsen, *Nano Lett.* **2016**, *16*, 4368.
[210] W. Liu, B. Lee, C. H. Naylor, H. S. Ee, J. Park, A. T. C. Johnson, R. Agarwal, *Nano Lett.* **2016**, *16*, 1262.
[211] D. Zheng, S. Zhang, Q. Deng, M. Kang, P. Nordlander, H. Xu, *Nano Lett.* **2017**, *17*, 3809.
[212] X. Liu, W. Bao, Q. Li, C. Ropp, Y. Wang, X. Zhang, *Phys. Rev. Lett.* **2017**, *119*, 027403.
[213] B. Lee, W. Liu, C. H. Naylor, J. Park, S. C. Malek, J. S. Berger, A. T. C. Johnson, R. Agarwal, *Nano Lett.* **2017**, *17*, 4541.
[214] C. Schneider, M. M. Glazov, T. Korn, S. Höfling, B. Urbaszek, *Nat. Commun.* **2018**, *9*, 2695.
[215] J. J. Baumberg, J. Aizpuruz, M. H. Mikkelsen, D. R. Smith, *Nat. Mater.* **2019**, https://doi.org/10.1038/s41563-019-0290-y
[216] K. L. Koshelev, S. K. Sychev, Z. F. Sadrieva, A. A. Bogdanov, I. V. Iorsh, *Phys. Rev. B* **2018**, *98*, 161113(R).
[217] J. Flick, N. Rivera, P. Narang, *Nanophotonics* **2018**, *7*, 1479.
[218] A. Majumdar, C. M. Dodson, T. K. Fryett, A. Zhan, S. Buckley, D. Gerace, *ACS Photonics* **2015**, *2*, 1160.
[219] Y. Li, J. Zhang, D. Huang, H. Sun, F. Fan, J. Feng, Z. Wang, C. Z. Ning, *Nat. Nanotechnol.* **2017**, *12*, 987.
[220] D. Neshev, I. Aharonovich, *Light: Sci. Appl.* **2018**, *7*, 58.
[221] T. T. Tran, D. Wang, Z.-Q. Xu, A. Yang, M. Toth, T. W. Odom, I. Aharonovich, *Nano Lett.* **2017**, *17*, 2634.
[222] S. Wu, S. Buckley, J. R. Schaibley, L. Feng, J. Yan, D. G. Mandrus, F. Hatami, W. Yao, J. Vučković, A. Majumdar, *Nature* **2015**, *520*, 69.
[223] Y. Ye, Z. J. Wong, X. Lu, X. Ni, H. Zhu, X. Chen, Y. Wang, X. Zhang, *Nat. Photonics* **2015**, *9*, 733.